TITLE

Chromatin remodeling initiates transcriptional and post-transcriptional silencing in *Neurospora*

AUTHORS

Florian Carlier*, Sebastian Castro Ramirez*, Jaafar Kilani, Sara Chehboub, and Eugene Gladyshev**

AFFILIATIONS

Institut Pasteur, Université Paris Cité, Molecular Genetics and Epigenetics Unit, F-75015 Paris, France

* Equal contribution

** Correspondence: eugene.gladyshev@gmail.com

ABSTRACT

In many eukaryotes, including mammals, transcriptional (heterochromatin-mediated) and post-transcriptional (RNAi-mediated) silencing of repetitive DNA can be initiated by poorly understood mechanisms independent of strong sequence-specific cues. We found that in the fungus *Neurospora crassa* both types of silencing were induced by the aberrant binding of transcription factors to a synthetic repetitive locus represented by the *tetO* operator array. Transcriptional silencing of the array was mediated by canonical constitutive heterochromatin. On the other hand, post-transcriptional silencing resembled quelling, but occurred normally in the absence of RAD51 and RAD52, two principal recombination factors. Therefore, this process was named recombination-independent quelling (RIQ). Initiation of RIQ and heterochromatin was associated with perturbed chromatin, and both processes required SAD-6, a SWI/SNF chromatin remodeler orthologous to ATRX. Without SAD-6, and while still occupied by transcription factors, the locus featured an extreme state that was associated with strong nucleosome depletion and high MNase sensitivity, however, this state was unable to promote silencing. We also found that native AT-rich DNA (which comprises relics of transposable elements in *N. crassa*) could undergo RIQ according to the same principles. These results suggested a general model in which the *de novo* silencing can be induced by the active remodeling of a perturbed (nucleosome-depleted) chromatin state.

KEYWORDS

Transcriptional gene silencing; post-transcriptional gene silencing; repeat-induced gene silencing; quelling; constitutive heterochromatin; nucleosome-depleted regions; chromatin remodeling; operator arrays; AT-rich DNA; TetR; GATA factors; ATRX; SAD-6; *Neurospora*

INTRODUCTION

The genomes of most eukaryotes contain large amounts of repetitive DNA silenced transcriptionally and post-transcriptionally by diverse mechanisms. Some of these mechanisms employ strong sequence-specific signals to select their targets. For example, in animals, dispersed copies of mobile genetic elements are recognized by KRAB domain-containing zinc finger proteins (KZFPs) that recruit the methyltransferase SETDB1 and other factors to initiate heterochromatin assembly [1]. In parallel, in the animal germline, transcripts of such repeats become targeted by complementary piRNAs capable of guiding potent transcriptional and post-transcriptional repression [1].

In other cases, a threshold number of tandem repeats (including pericentromeric, telomeric, and microsatellite DNA) is required to induce silencing [2,3]. This thresholding principle also applies to gene arrays, such as the human D4Z4 array carrying *DUX4* genes [4]. A pathological contraction of this array relieves the silencing of *DUX4*, resulting in type 1 facioscapulohumeral muscular dystrophy (FSHD1) [4]. This type of silencing is not limited to native sequences, and can also affect transgenic arrays made of foreign DNA. Such process, known as repeat-induced gene silencing (RIGS), was documented in fungi [5], plants [6], and animals [7,8]. Notably, in mammals, a screen for regulators of RIGS identified a number of factors also required for heterochromatin assembly at native gene arrays (such as SMCHD1, a non-canonical member of the structural maintenance of chromosomes protein family) [9,10], suggesting that the underlying mechanisms could be broadly conserved. Yet the nature of these mechanisms remained unknown.

ATRX (Alpha Thalassemia/Mental Retardation Syndrome X-Linked) is a member of the SWI/SNF family of chromatin remodelers [11]. In a complex with the histone chaperone DAXX, ATRX was shown to deposit the histone variant H3.3 at several types of repetitive sequences (pericentromeric, telomeric, ribosomal and other repeats) as well as some non-repetitive regions [11]. H3.3 deposited by ATRX-DAXX often carries H3K9me3 [11]. Overall, ATRX is involved in diverse chromatin-based processes that include transcriptional silencing of repetitive DNA, telomere maintenance, recombinational DNA repair, resolution of secondary DNA structures, and regulation of gene expression [11]. In addition to DAXX, ATRX can interact with other chromatin factors (proteins and long noncoding RNAs) as well as specific histone modifications H3K9me3 and H3K4me0 [11]. ATRX is also known for its ability to recognize and remodel nucleosome-depleted chromatin associated with atypical transcription, including the Hsp70 genes during heat shock in Drosophila [12] and GC-rich telomeric repeats giving rise to R-loops [13].

The model fungus *Neurospora crassa* sports several processes that involve the *de novo* initiation of silencing, both transcriptional and post-transcriptional. With respect to transcriptional silencing, first, in vegetative cells,

newly integrated transgenic repeats were reported to become heavily methylated, as the result of potent RIGS [5]. Second, during sexual phase, all duplications of chromosomal DNA longer than a few hundred base-pairs (with the exception of ribosomal DNA) become subject to strong repeat-induced point mutation (RIP), during which many cytosines in repeats are converted to thymines [14,15]. Importantly, RIP can be carried out by the same pathway that establishes *de novo* DNA methylation during RIGS [5,16].

Concerning the initiation of post-transcriptional silencing, two processes need to be considered. One process, known as quelling, triggers the expression of small interfering RNAs (siRNAs) from repetitive transgenes in vegetative cells [17]. Another process, known as meiotic silencing by unpaired DNA (MSUD), takes place in early meiosis and triggers the expression of siRNAs from the mismatching loci found at the allelic positions on pairs of homologous chromosomes [18,19]. Whereas MSUD occurs normally without DNA breakage and recombination [20], quelling was proposed to rely on recombinational DNA repair as a mechanism for repeat recognition [21]. Interestingly, potent MSUD was shown to require SAD-6, a fungal ortholog of ATRX [22].

A sizable portion of the *Neurospora* genome corresponds to AT-rich DNA, which comprises relics of repeats (mutated by RIP) that become subject to transcriptional (mediated by constitutive heterochromatin) and post-transcriptional silencing [23]. Studies focused on AT-rich chromatin provided a comprehensive understanding of constitutive heterochromatin assembly in *N. crassa* [23]. Specifically, it was established that all H3K9me3 (the characteristic mark of constitutive heterochromatin) is catalyzed by DIM-5, a lysine methyltransferase of the SUV39 family [23]. In its turn, H3K9me3 becomes recognized by HP1, which also forms a complex with DIM-2, a canonical cytosine methyltransferase responsible for all DNA methylation in *N. crassa* [23]. Thus, in this pathway, AT-rich DNA provides a hardwired signal for H3K9me3 and ensuing DNA methylation [23]. Many additional factors controlling H3K9me3 in this context were identified, including histone deacetylases and chromatin remodelers [24,25]. In parallel, a more dynamic type of DNA methylation was found at some loci associated with antisense transcription [26,27]. Interestingly, the latter phenomenon also requires DIM-5 and HP1, suggesting that the role of H3K9me3 in directing DNA methylation has been broadly conserved in *N. crassa* [28]. Yet, it remains unclear how H3K9me3 can be established *de novo* in this and other situations (including RIP and RIGS) independent of strong sequence-specific cues.

This study was motivated by several considerations. First, in *Neurospora*, a synthetic *tetO* operator array was shown to activate RIP by the heterochromatin-related pathway, suggesting that such a construct could initiate transcriptional silencing *de novo* [29]. Second, in budding yeast, the association of such operator arrays with their corresponding repressor proteins (LacI or TetR) was also shown to induce transcriptional silencing of a nearby reporter [30,31]. This process started with phosphorylation and concomitant depletion of histone H2A,

suggesting that the tight binding of repressor proteins led to chromatin stress and nucleosome loss; and it did so by a mechanism independent of DNA replication [30]. The perturbed array was directed to the perinuclear compartment, where it became gradually occupied by Silent Information Regulator (SIR) proteins, the critical effectors of transcriptional silencing in budding yeast [30]. At the end, the heterochromatinized array featured stabilized nucleosomes and had its overall accessibility reduced [30]. With respect to a possible mechanism, it was proposed that the tight yet dynamic binding of multiple repressor molecules could accelerate nucleosome turnover and promote the incorporation of new histones without certain modifications which would normally interfere with the recruitment of the SIR proteins [30].

We found that the *lacO* and *tetO* arrays could be silenced in vegetative cells of *N. crassa* transcriptionally (by constitutive heterochromatin) and post-transcriptionally (by RNAi). At the *tetO* array, the silencing could be induced by the aberrant binding of TetR-GFP or NIT-2 (a conserved transcription factor of the GATA family). In both situations, the chromatin state of the array became perturbed. Post-transcriptional silencing resembled quelling, however, it occurred normally even if homologous recombination was inactivated genetically. Thus, we named this process 'recombination-independent quelling' (RIQ). Critically, both heterochromatin assembly and RIQ of the perturbed *tetO* array required SAD-6. When still bound by transcription factors in the absence of SAD-6, the array assumed an open state associated with very strong nucleosome depletion and high MNase sensitivity, yet it was not competent for silencing. Importantly, we found that AT-rich DNA could also undergo RIQ according to the same principles. Taken together, our results led to a general model in which the *de novo* silencing can be initiated by the active remodeling of a perturbed (nucleosome-depleted) chromatin state.

RESULTS

Binding of TetR-GFP to the *tetO* array induces constitutive heterochromatin and sRNA expression

In budding yeast, the tight binding of TetR or LacI proteins to their corresponding operator arrays can trigger transcriptional silencing of a nearby reporter gene [31]. It was interesting to test if a similar process occurred in *N. crassa*, an organism with canonical transcriptional (heterochromatin-mediated) and post-transcriptional (RNAi-mediated) silencing [23]. To this end, the state of chromatin was assayed by ChIP-seq and MNase-seq, while RNAi was analyzed by sRNA-seq, focusing on sRNAs with the 5' phosphate and the free 3' OH groups.

Standard *lacO* and *tetO* arrays were used in this study [32]. The arrays included 168 *lacO1* and 191 *tetO* sites and were characterized by GC-content of ~40% and ~50%, respectively (Fig. S1A). The *lacO* array featured three perfect repeats of several hundred base-pairs, whereas the *tetO* array was devoid of such elements (Fig. S1A). The arrays were concatenated on a plasmid and integrated by homologous recombination into Strain O to produce Strain A (Fig. 1A). Subsequently, the *csr-1+* gene in Strain A was replaced with *tetR-gfp* to create

Strain B (Fig. 1A). In this latter strain, a synthetic variant of the TetR repressor (TetR-GFP) was expected to associate with the *tetO* array throughout the cell cycle [29]. This interaction could be disrupted by culturing *N. crassa* in the presence of tetracycline [29].

We started by analyzing the state of the *lacO–tetO* locus in Strain A, grown in the standard minimal medium. In this situation, no above-background expression of array-derived sRNAs could be detected (Fig. 1C,G) At the same time, a prominent peak of heterochromatin was found at the *lacO* array (Fig. 1B). The AT-rich motif ATAACAATT was noted in the sequence of *lacO1* (Fig. S1A). This motif could potentially constitute a signal for heterochromatin assembly by a mechanism that normally silences AT-rich DNA in *N. crassa* [23].

Two striking outcomes were observed in the presence of TetR-GFP (in Strain B). First, the *tetO* array became heavily heterochromatic (Fig. 1B). Second, the *tetO* array also started to express massive amounts of sRNAs (Fig. 1C,G). These *tetO*-derived sRNAs were mainly 20-23 nt in length, with a strong bias for uracil at the 5' position (Fig. 1D). Both silencing processes were completely suppressed by growing Strain B in the presence of tetracycline (Fig. 1B,C,G). These results suggested that the aberrant binding of TetR-GFP to the *tetO* array could initiate potent transcriptional and post-transcriptional silencing in *N. crassa*.

Expression of sRNAs can be modulated by long-range effects

While TetR-GFP induced the strongest RNAi response at the *tetO* array, the upregulated expression of sRNAs could be detected at some sites as far as 100 kbp away from the repressor-bound locus (Fig. 1E). The majority of such loci were non-coding. This intriguing effect may involve repositioning of the repressor-bound array to another territory (as it occurs in budding yeast [30]), or having the array acquired enhancer-like properties, for example, by recruiting (and thus concentrating) a critical silencing factor in its vicinity [33].

A set of endogenous sRNA loci provides a standard reference for comparative sRNA-seq analysis

To compare levels of array-derived sRNAs between different conditions, a group of endogenous sRNA loci was designated as a standard reference. Such loci exhibited strong and invariant patterns of expression, with the majority of them corresponding to tRNA and 5S RNA genes (examples are shown in Fig. S1B). For the purpose of the analysis, these loci were represented by 463 500-bp tiles (tile coordinates are provided in SI Data File 3). For any given condition, the standard level was estimated as the median number of sRNA reads mapped to those reference tiles. This value was then used to normalize and compare levels of array-derived sRNAs (calculated as the median number of reads mapped to the tiles covering the arrays). Our analysis also indicated that the designated reference set was useful in comparing sRNA datasets between studies based on different strains and library construction protocols (Fig. S1C).

The *lacO–tetO* locus undergoes recombination-independent quelling (RIQ)

In *N. crassa*, the expression of sRNAs from repetitive transgenes represents a hallmark of quelling [17]. Thus, we asked if the expression of sRNAs from the *tetO* array required the three canonical quelling factors, QDE-1 (RNA-dependent RNA polymerase), QDE-2 (Argonaute protein) and QDE-3 (RecQ/Sgs1 helicase). We found that QDE-1 was absolutely essential for the biogenesis of *tetO*-derived sRNAs, while a small amount of *tetO*-derived sRNAs could still be detected in the absence of QDE-3 (Fig. 1F,G). We confirmed that the *tetO* array remained bound by TetR-GFP in those conditions (Fig. S2B). On the other hand, in the absence of QDE-2, the apparent levels of *tetO*-derived sRNAs were mildly elevated; and a similar trend was observed in the absence of the exonuclease ERI1, which was implicated in heterochromatin formation and sRNA expression linked to antisense transcription [34] (Fig. 1F,G). Notably, the expression of *lacO*-derived sRNAs also required QDE-1 and QDE-3, but not QDE-2 or ERI1 (Fig. 1F,G). These results suggested that all array-derived sRNAs were produced by a process that resembled canonical quelling.

Earlier studies linked quelling with homologous recombination in *N. crassa* [21]. Thus, we asked if the newly uncovered quelling-like process required RAD51 and RAD52, the two critical recombination factors. Several results were observed in the absence of RAD51 or RAD52. First, the expression of *tetO*-derived sRNAs was not affected, revealing a recombination-independent nature of this system (Fig. 1F,G). Second, the expression of sRNAs from (sub)telomeric regions increased substantially. This effect manifested itself as a characteristic arch on the scatter plots (Fig. 1G, red arrows), and also as a series of large peaks on the genome-wide maps of normalized sRNA-seq counts (Fig. S3C). Third, we also observed a peculiar increase in 'background' sRNAs, expressed normally at low levels throughout the genome [35] (Fig. 1G; Fig. S3C). This effect was manifested as a rightward shift at the base of the scatter relative to the reference loci (Fig. 1G). Fourth, the loss of RAD51 or RAD52 was associated with an apparent mild increase in *lacO*-derived sRNAs (Fig. 1F,G). With respect to the magnitude of these effects, deleting *rad52+* had a greater impact in comparison to deleting *rad51+*.

Taken together, our results conjectured two critical points. First, in *N. crassa*, similarly to budding yeast [31], the repressor-bound *tetO* array induced transcriptional silencing. Second, the same locus also became subject to potent post-transcriptional silencing, which resembled quelling yet occurred normally even if homologous recombination was disabled. This latter process was named recombination-independent quelling (RIQ).

Type I topoisomerase TOP3 (the canonical partner of QDE-3) is dispensable for RIQ

Sgs1 (the yeast ortholog of QDE-3) partners with the type I topoisomerase Top3 to form a conserved complex involved in several aspects of recombinational DNA repair [36]. Thus, we asked if the *Neurospora* ortholog of

Top3 had a role in RIQ. We found that the *top3Δ* condition was associated with a 6-fold decrease in the levels of *tetO*-derived sRNAs, which was paralleled by a 10-fold *increase* in the levels of *lacO*-derived sRNAs (Fig. 1F,G). Genome-wide, the *top3Δ* condition was also associated with the elevated levels of background sRNAs, whereas subtelomeric sRNAs remained unaffected (Fig. 1G). The increased expression of background sRNAs was evidenced by having many sRNA-seq reads mapped to *his-3* and *lpl*, two genes flanking the arrays (Fig. S3B). These results suggested that QDE-3 mediated RIQ by a mechanism that did not involve TOP3.

Acetyltransferase RTT109 is important for RIQ

In *Neurospora*, expression of some sRNA species requires the acetyltransferase RTT109 [37], which catalyzes acetylation of lysine-56 on histone H3 to control nucleosome dynamics coupled to DNA replication and repair [38]. Therefore, we investigated if RTT109 was required for RIQ. To this end, a 52-fold decrease in the levels of *tetO*-derived sRNAs was observed in the *rtt109Δ* strain (Fig. 1F,G). At the same time, *lacO*-derived sRNAs were not affected (Fig. 1F,G). Globally, the loss of RTT109 resembled the recombination-deficient condition, including the characteristic upregulation of subtelomeric and background sRNAs (Fig. 1G; Fig. S3C). These results suggested that RTT109 exerted its role in RIQ through its control of replication-dependent nucleosome homeostasis.

Heterochromatin assembly during RIQ is both RNAi- and recombination-independent

Our ChIP-seq analysis of the relevant mutant conditions produced several insights. First, the arrays remained fully heterochromatic in the absence of either QDE-1, QDE-2, QDE-3, ERI1, RAD51 or RAD52 (Fig. S2A). These results corroborated pioneering reports of RNAi-independent heterochromatin assembly in *Neurospora* [39,40]. Second, at the *tetO* array, the levels of histone H3 were decreased in the presence of TetR-GFP (Fig. 1B; Fig. S2C). This result was important, because it suggested that RIQ could be associated with a perturbed chromatin state. Third, in the absence of RTT109, the arrays became less heterochromatic, while the levels of hH3 remained the same (Fig. S2A,C,D). This specific result suggested that the acetyltransferase RTT109 had a role in heterochromatin assembly in *N. crassa*, as also reported earlier in fission yeast [41].

The latter results were obtained by plotting normalized log10-transformed ChIP-seq counts (or their ratios) as a function of GC-content. This approach proved to be informative, in part, because the genome of *N. crassa* is characterized by a bimodal GC-content distribution (Fig. S1D). In this situation, the two classes of sequences correspond to essentially independent moieties associated with distinct molecular properties. Representing the genome as a set of non-overlapping 500-bp tiles allowed us to use the resulting bias-free genome-wide data as a reference frame, with respect to which the properties of the arrays could be understood. This approach was extended to the analysis of sRNA-seq data as well.

RIQ is constrained by heterochromatin

We next asked if the expression of array-derived sRNAs was constrained by heterochromatin. To this end, we discovered that the arrays lost their heterochromatic character in the absence of the histone deacetylase HDA1 (Fig. S2A). At the *lacO* array and many AT-rich regions, this effect was paralleled by a strong decrease in the hH3 occupancy (Fig. S2C). With respect to sRNAs, two results were observed. First, levels of *tetO*- and *lacO*-derived sRNAs surged by a factor of 18 and 539, respectively (Fig. 1F,G). Second, the expression of sRNAs was also strongly upregulated at a number of AT-rich loci (Fig. 1G; Fig. S2A, blue arrows). The derepressed AT-rich loci were found throughout the genome, with a tendency to concentrate on Chromosome I (Fig. S3C). Among all conditions associated with large-scale changes in sRNA expression tested thus far (Fig. S3A), such a strong effect was only observed in the absence of HDA1. We note that a similar result was described earlier in *Neurospora* strains lacking all heterochromatin [42]. Taken together, these results advanced the notion that the expression of some sRNAs was constrained by heterochromatin in *N. crassa*.

Conserved chromatin remodeler CHD1 is not required for RIQ

An emerging connection between perturbed chromatin and RIQ encouraged us to investigate the involvement of chromatin remodeling factors. We started by testing CHD1 (Chromodomain Helicase DNA Binding Protein 1), which was already implicated in regulation of transcriptional [26] and post-transcriptional [21] silencing in *Neurospora*. We found that the deletion of *chd1+* had no effect on the levels of hH3 or heterochromatin at the arrays (Fig. S4A,C,D). To a first approximation, the levels of array-derived sRNAs remained the same as well (Fig. S4B). These results suggested that CHD1 did not play any role in silencing in this system.

SAD-6 controls all silencing of the repressor-bound *tetO* array

Our results indicated that RIQ resembled MSUD in being independent of recombination. Thus, we asked if SAD-6, a critical MSUD factor, was involved in RIQ. Several striking observations were made. First, all RIQ and heterochromatin at the repressor-bound *tetO* array were eliminated in the absence of SAD-6 (Fig. 2A,B; Fig. S5A). Second, these effects were accompanied by a dramatic decrease in the hH3 occupancy, which was restored by growing the *sad-6Δ* strain in the presence of tetracycline (Fig. 2B). Third, the same dynamics was also exhibited by histone H2B (Fig. 2D). Fourth, in the series 'Strain A > Strain B > Strain B: *sad-6Δ*', the loss of histones at the *tetO* array was paralleled by a strong increase in MNase sensitivity (Fig. 2C,E; Fig. S2C).

The genome-wide comparison of Strain B and 'Strain B: *sad-6Δ*' yielded several additional insights. First, the loss of hH2B and hH3 in the *sad-6Δ* condition was limited to the *tetO* array and possibly rDNA (Fig. S5B,G). The latter result was provocative, but it was not pursued in this study. Second, following the loss of histones,

the repressor-bound *tetO* array represented an unusual strongly nucleosome-depleted region (SNDR), being the only genomic locus with more than 6 consecutive SNDR tiles (defined by having the log10-transformed (IP[hH3]+1)/(Input+1) ratio of -0.5 or less) (Fig. 2E; Fig. S5D). Third, without SAD-6, heterochromatin was lost at the total of three sites, including the array, rDNA, and a region upstream of NCU03868, designated as '*r2*' (Fig. S5G,K). In this region, heterochromatin was eliminated specifically between two blocks of AT-rich DNA (Fig. S5K). Fourth, the *tetO* array was the only genomic site marked by a substantial increase in MNase sensitivity (Fig. S5C,H). Fifth, only one additional locus (spanning a 17-kbp interval between NCU00748 and NCU00751, and designated as '*r1*') was associated with a strong reduction in sRNA expression in the *sad-6Δ* condition (Fig. S5F,J). Normally, this region produced sRNAs from both strands (Fig. S5J) by a process that required QDE-1 (Fig. S3C).

SAD-6 is recruited to perturbed chromatin

To test if SAD-6 regulated the state of the *tetO* array directly, we replaced the promoter of the native *sad-6+* gene with a construct that provided an N-terminal FLAG tag and also increased the expression of the tagged SAD-6 protein, to compensate for a partial loss of its activity (Fig. S5E). This system allowed us to make the following observations. First, in the presence of TetR-GFP, FLAG-SAD-6 became highly enriched at the *tetO* array, where it remained partially active (as evidenced by the intermediate levels of hH3 and heterochromatin over the array, Fig. 1B; Fig. 2F). Second, the association of FLAG-SAD-6 with the *tetO* array was disrupted by tetracycline, which inactivated the repressor (Fig. 2F). Third, genome-wide, comparable enrichment levels were only found at one additional locus (designated as '*r3*'), which overlapped the promoter of NCU01783 (a putative phosphatidylinositol N-acetylglucosaminyltransferase, Fig. S5I,L). The latter effect was unexpected yet reproducible (Fig. S5L). Taken together, these results suggested that the *tetO* array, in its perturbed state, represented a particularly favorable substrate for SAD-6.

Overall, our results advanced three main points. First, the binding of TetR-GFP to the *tetO* array generated a state of perturbed chromatin and triggered robust transcriptional and post-transcriptional silencing. The latter process resembled quelling, yet it occurred normally in the absence of the two critical recombination factors, RAD51 and RAD52. Second, SAD-6 (a SWI/SNF chromatin remodeler orthologous to ATRX) emerged as a principal regulator of all silencing in this system. Third, when bound by TetR-GFP in the absence of SAD-6, the array featured an open state associated with strong nucleosome depletion and high MNase sensitivity; yet, this state was not competent for silencing. Instead, it likely constituted a *bona fide* substrate for SAD-6.

Transcription factor NIT-2 mediates all silencing of the *tetO* array induced by nitrogen starvation

Our results suggested that the aberrant binding of TetR-GFP perturbed the state of chromatin at the *tetO* array

and promoted the onset of silencing. It was critical to know if the role played by TetR-GFP in this system was general. If so, TetR-GFP could be substituted by an analogous yet unrelated factor. Here we took advantage of the fact that each *tetO* site contains two 'GATA' motifs (Fig. S1A) known to recruit GATA factors *in vivo* [43]. In *Neurospora*, upon nitrogen starvation, the GATA factor NIT-2 activates the expression of genes involved in nitrogen metabolism [44]. The DNA binding domain of NIT-2 is highly conserved (Fig. 3A), and its capacity to recognize the core GATA sequence was validated *in vitro* [44]. Whereas only a few GATA motifs are found in the promoters of genes directly regulated by NIT-2 [45] (Fig. 3B), the presence of hundreds of GATA sites in the *tetO* array could create a situation in which the aberrant binding of many NIT-2 molecules could perturb chromatin analogously to TetR-GFP.

To investigate the function of NIT-2 at the *tetO* array, the latter was transformed into Strain O to create Strain E (which was otherwise isogenic to Strain B). The experimental procedure included pre-growing *Neurospora* in the standard minimal medium for 24 hours, after which mycelial sample was rinsed, transferred into a new medium lacking all nitrogen, grown for additional 5 hours, and harvested for analyses (Fig. 3C). This protocol focused on the short-term effects and permitted testing relevant factors during the earliest stages of silencing.

We first confirmed that the *tetO* array was competent for silencing in the absence of the adjoining *lacO* array. To this end, we transformed *tetR-gfp* into Strain E and found that, upon being provided with the repressor, the lone *tetO* array assembled heterochromatin and induced RIQ at the levels similar to the *tetO* array in Strain B (Fig. 3D). These results showed that the *tetO* array was autonomous with respect to the remodeling-dependent silencing.

Remarkably, subjecting Strain E to nitrogen starvation for only 5 hours recapitulated the effects produced by the constitutive binding of TetR-GFP (Fig. 3D). First, the *tetO* array became fully heterochromatic (Fig. 3D). Second, the *tetO* array also started to express large amounts of sRNAs (Fig. 3D). Indeed, the levels of sRNAs induced by starvation versus TetR-GFP were very similar (Fig. 3D). To determine if NIT-2 was necessary for the initiation of silencing in this system, we deleted *nit-2+* and subjected the mutant to starvation. No sRNA expression or heterochromatin could be detected at the *tetO* array in this situation (Fig. 3D,E), demonstrating that NIT-2 was indeed absolutely essential for all starvation-induced silencing of the *tetO* array.

Several additional insights were obtained. First, because the expression of those *tetO*-derived sRNAs required QDE-1 and QDE-3 but not RAD51 or RAD52 (Fig. 3E), it was classified as RIQ. Notably, while the levels of *tetO*-derived sRNAs declined nearly 8-fold in the absence of RAD52, they were still two orders of magnitude above background (Fig. 3E). Second, heterochromatin was formed normally in the absence of QDE1, QDE-3,

RAD51 and RAD52 (Fig. S6A). This result excluded the roles of RNAi and recombination in the initiation of transcriptional silencing at the *tetO* array. Third, genome-wide, sRNA expression increased upon starvation at several additional loci (Fig. S6B). For some of them, the effect was also dependent on NIT-2 (Fig. S6B).

SAD-6 controls all starvation-induced silencing

Thus far, our results suggested that the silencing induced by nitrogen starvation (and mediated by NIT-2) was equivalent to the silencing induced by TetR-GFP. Subsequent experiments established that the corresponding *sad-6Δ* conditions were also equivalent (Fig. 3D-I). Specifically, the following outcomes were observed upon nitrogen starvation in the absence of SAD-6. First, *tetO*-derived sRNAs were essentially eliminated (Fig. 3D). Second, levels of hH2B and hH3 became diminished, once again turning the *tetO* array into an exceptionally large SNDR (Fig. 3D,F-H). Third, no heterochromatin was formed (including in the region containing *GmR*, where nucleosomes were still apparently present, Fig. 3D). Fourth, the *tetO* array became extremely sensitive to MNase (Fig. 3I). Fifth, genome-wide, the array was essentially the only genomic locus associated with the aforementioned chromatin defects (Fig. S6C,D).

Taken together, our results established that TetR-GFP and NIT-2, two dissimilar transcription factors (broadly defined), could activate silencing in a similar way. In both situations, the aberrant binding of these proteins to the *tetO* array induced a state of perturbed chromatin, which was remodeled by SAD-6. The silencing became induced as a result of this remodeling activity. In addition, our results suggested that, in the wildtype situation, the *tetO* array represented the only genomic locus subject to such repression, implying that *N. crassa* evolved to avoid sustained activation of the remodeling-dependent silencing at endogenous sequences.

DNA replication is required for starvation-induced RIQ

Our results showed that strong RIQ of the *tetO* array required the acetyltransferase RTT109, suggesting a link with DNA replication (Fig. 1F,G). On the other hand, canonical quelling was also shown to become repressed by 0.1M hydroxyurea (HU) [46], a potent yet reversible inhibitor of DNA replication in *N. crassa* [47]. Thus, we asked if DNA replication was required for RIQ. Focusing on Strain B, we found that *tetO*-derived sRNAs were downregulated 7-fold after a prolonged incubation of mycelia in the growth medium supplemented with 0.1M HU (Fig. 1F,G). This result indicated that RIQ was promoted by DNA replication. Yet, because HU was added to the pre-grown cultures, in which RIQ was fully active, and because the ensuing loss of array-derived sRNAs depended on their stability (an unknown parameter), the true magnitude of the inhibitory effect of HU on RIQ remained unclear.

The above question was addressed using an experimental system provided by starvation-induced RIQ (Fig. 4).

To arrest all DNA replication prior to starvation, HU was first added during the last 5 hours of normal growth (Fig. 4A). This block could be either released or maintained in the nitrogen-free medium (Fig. 4A). We found that starvation-induced RIQ was completely and specifically inactivated if the HU block was maintained (Fig. 4B). The only other sRNAs downregulated in this situation were those produced from AT-rich DNA (Fig. 4C). These results demonstrated that DNA replication was critical for starvation-induced RIQ of the *tetO* array.

The *lacO* array and native AT-rich DNA can undergo RIQ

The expression of sRNAs from AT-rich DNA was intriguing. As reported previously, such sRNAs began with uracil and were suppressed by constitutive heterochromatin [35,42]. Our results suggested that native AT-rich DNA and the *lacO* array shared several properties, including the occurrence of AT-rich motifs and the related ability to induce constitutive heterochromatin. In addition to constitutive heterochromatin, *N. crassa* features facultative heterochromatin marked by H3K27me3, which is deposited by the lysine methyltransferase SET-7, an ortholog of E(Z) [23]. Compromised viability of *dim-5Δ* strains can be restored by deleting *set-7+* [42,48]. Thus, to analyze expression of sRNAs from the *lacO* array and AT-rich DNA, we moved the *lacO–tetO* locus to a new genetic background (Strain C, made by a cross), in which *dim-5+* and *set-7+* were both deleted (Fig. 5A). A corresponding isogenic *dim-5+* strain ('Strain C: *dim-5+*', also called Strain D, Fig. 5A) was made by replacing *csr-1+* in Strain C with the *dim-5+* transcription unit [16].

Several insights concerning the role of DIM-5 at AT-rich chromatin were obtained by comparing Strain C with 'Strain C: *dim-5+*'. First, large amounts of sRNAs were produced from the *lacO* array and AT-rich DNA when DIM-5 was absent (Fig. 5B,E,F; Fig. S7A,B). Second, the affected regions also exhibited a visible decrease in the hH3 occupancy (Fig. 5C). As the result, with respect to the levels of hH3 and sRNAs, the state of the *lacO* array in Strain C became analogous to that of the *tetO* array in Strain B. Our further analysis showed that the expression of sRNAs from the *lacO* array and AT-rich DNA required QDE-1 but not RAD51 (Fig. 5D-F; Fig. S7B,H). The roles of QDE-3 and RAD52 could not be evaluated, because we were unable to delete *qde-3+* or *rad52+* in this genetic background (Strain C). Importantly, those sRNAs were downregulated by the treatment with HU in a manner similar to *tetO*-derived sRNAs in Strain B (Fig. S7B,C; Fig. 1G). Taken together, these results implied that the *lacO* array and AT-rich DNA, when stripped of heterochromatin, assumed a perturbed chromatin state associated with RIQ.

SAD-6 regulates RIQ of AT-rich DNA

Regarding the role of SAD-6 in RIQ of AT-rich DNA, two principal results were observed. First, the majority of the AT-rich loci upregulated in the absence of heterochromatin had their expression levels decreased in the *sad-6Δ* condition; yet, this effect was not absolute (Fig. 5D-F). Second, the loss of SAD-6 was also paralleled

by a broad increase in MNase sensitivity of AT-rich DNA (Fig. 5G; Fig. S7G). This effect was not observed in Strain B, where AT-rich DNA was heterochromatinized (Fig. S5C). For the majority of those sRNA-producing AT-rich loci, the increase in MNase sensitivity was modest and largely uniform, yet some sites featured larger changes (Fig. 5G). Taken together, these results suggested that RIQ of AT-rich DNA, analogous to RIQ of the *tetO* array, was regulated by SAD-6 or/and a similar chromatin remodeling activity.

The *lacO* array becomes genetically unstable in the absence of heterochromatin

We found that *lacO*-derived sRNAs were still expressed promptly without SAD-6 (Fig. S7H). This result was not entirely surprising, as SAD-6 was partially dispensable for RIQ of AT-rich DNA. However, in this *sad-6Δ* strain, a large deletion in the *lacO* array was detected (Fig. S7H). Because such deletions were never observed in Strain B and its *sad-6Δ* derivative, this result implied that the *lacO* array became genetically unstable when stripped of heterochromatin. To test this idea, we employed a multiplex PCR approach to detect the loss of the central portion of each array in a clonal population of nuclei (Fig. S8A). In this assay, the first pair of primers amplified the central part of each array containing a drug resistance marker (Fig. S1A), while the second pair was used to amplify the *spo11* gene, as the positive control (Fig. S8B). By this approach, frequent deletions in the *lacO* array were observed specifically in the absence of heterochromatin (Fig. S8B). Our further analysis indicated that all these deletions were associated with the three perfect repeats present in the *lacO* array (Fig. S1A). Thus, while both arrays could undergo RIQ linked to perturbed chromatin, the *lacO* array was different from the *tetO* array in featuring marked genetic instability in its perturbed state.

HDA1 and CHAP, two members of the HCHC complex, play contrasting roles in RIQ of the *lacO* array

We next analyzed the role of constitutive heterochromatin in RIQ of the *lacO* array. In *N. crassa*, constitutive heterochromatin is controlled by several protein complexes, most notably by DCDC and HCHC [23]. DCDC establishes H3K9me3 and contains DIM-5 (the catalytic subunit), DIM-7, DIM-9, CUL4, and DDB1; while HCHC mediates histones deacetylation and contains HDA1 (the catalytic subunit), along with HP1, CDP-2, and CHAP [23]. With respect to DCDC, out results indicated that the deletions of *dim-7+* and *dim-9+* erased constitutive heterochromatin and activated RIQ in a manner similar to the deletion of *dim-5+* (Fig. S7D,E).

With respect to HCHC, a more complex outcome was observed. First, in the absence of HDA1, the *lacO* array entered a state related to the DCDC-deficient condition: (i) heterochromatin became nearly eliminated, (ii) the level of hH3 was reduced, and (iii) RIQ was strongly activated (Fig. S7D-F). Genome-wide, the levels of hH3 were also reduced at AT-rich DNA; yet, this effect was weaker than in 'Strain B: *hda1Δ*' (Fig. S2C; Fig. S7F). Second, in the absence of CHAP, the *lacO* array remained heterochromatinized, yet it also expressed sRNAs, albeit at a level an order of magnitude less compared to the *hda1Δ* condition (Fig. S7D,E). A modest decrease

in the hH3 occupancy was also observed (Fig. S7D,F). These results suggested that HDA1 and CHAP played different roles at the *lacO* array: whereas HDA1 acted as a critical factor in heterochromatin assembly, CHAP interfered with RIQ without apparently contributing much to the heterochromatic state of the *lacO* array.

At the *lacO* array, RIQ can be decoupled from heterochromatin assembly

Our results showed that the *lacO* array could (i) induce RIQ, (ii) form heterochromatin, and (iii) sustain high levels of genetic instability. It was important to know if those properties could be decoupled. To this end, we isolated two strains representing clonal lineages of Strain C, which carried spontaneous deletions in the *lacO* array of 5247 and 8263 bps (Fig. S9A). The corresponding truncated arrays (4454 and 1438 bps) were named *d(1)* and *d(2)*, respectively (Fig. S9A,B). Only *lacO.d(1)* could still activate RIQ (Fig. S9B). However, once DIM-5 was provided by transformation, *lacO.d(1)* and *lacO.d(2)* induced heterochromatin equally well (Fig. S9C). These results suggested that the capacity of the *lacO* array to activate RIQ could be decoupled from its capacity to induce heterochromatin.

In principle, *lacO.d(1)* could trigger RIQ because it contained some sequence motifs not present in *lacO.d(2)*. Alternatively, a threshold amount of *lacO* DNA could be required. To differentiate between these possibilities, we generated three new strains carrying overlapping 1.4-1.6 kbp fragments of *lacO.d(1)* (Fig. S9D,E). Neither fragment could trigger RIQ (Fig. S9F). However, these fragments induced heterochromatin equally well once DIM-5 was provided by transformation (Fig. S9G). These results suggested that the capacity to activate RIQ represented an emergent property of the *lacO* array, possibly mediated by a threshold-dependent mechanism.

DISCUSSION

The great diversity and abundance of repetitive DNA necessitate the evolution of different approaches to keep this fraction of the genome in check. While some of these approaches, including the KZFP-TRIM28-SETDB1 pathway in animals [1] and the RITS-CLRC relay in fission yeast [49], employ strong sequence-specific cues to silence low-copy repeats, others can promote silencing of only a large number of repeats organized as long tandem arrays [50]. The latter processes were proposed to rely on transcription-based mechanisms (involving R-loops, non-coding RNAs, and supercoiling) [50–52], homologous DNA-DNA pairing [16,53], and non-B-DNA structures [54,55]. Tandem repeats were also reported to frequently associate with non-histone proteins, such as transcription factors, which may exercise non-canonical roles in this context [50,56,57].

In this work, we have found that in the fungus *N. crassa*, transcriptional (heterochromatin-mediated) and post-transcriptional (RNAi-mediated) silencing can be induced by the aberrant binding of transcription factors to a model repetitive locus provided by the *tetO* array. The same effect was promoted by a synthetic variant of the

TetR repressor and an endogenous GATA factor NIT-2, suggesting that the general ability of such proteins to perturb chromatin (rather than to recruit a specific silencing activity) was a critical parameter. In its turn, the perturbed *tetO* array became recognized by the SWI/SNF chromatin remodeler SAD-6, which was absolutely essential for the initiation of all silencing in this system. While the transcriptional silencing was mediated by canonical constitutive heterochromatin, the post-transcriptional silencing resembled quelling, but proceeded normally in the absence of RAD51 and RAD52, two principal recombination factors. Therefore, this process was named recombination-independent quelling (RIQ).

Importantly, the properties of perturbed chromatin linked to RIQ of the *tetO* array were also relevant for RIQ of native AT-rich DNA. Thus, the state of perturbed chromatin has emerged as a general trigger of silencing in *Neurospora* (Fig. 6). The imperative role of chromatin remodeling stems from the fact that the perturbed state by itself could not trigger the silencing in the absence of SAD-6. In other words, the aberrant binding of many TetR-GFP or NIT-2 molecules to the *tetO* array and the resultant highly unusual perturbed state were invisible to the silencing machinery unless SAD-6 was allowed step in.

Recombination-independent quelling (RIQ)

At the *tetO* array, heterochromatin and RIQ were triggered concomitantly yet independently from one another. In principle, with respect to heterochromatin assembly, the function of SAD-6 may be analogous to the role of ATRX in the DAXX-dependent deposition of H3.3 [11]. On the other hand, the role of SAD-6 in RIQ (as well as MSUD [22]) appears profoundly mysterious.

Apart from quelling and MSUD, *N. crassa* has two more RNAi pathways capable of dynamically designating a new sRNA-producing locus [58]. The first (qiRNA) pathway is linked to DNA damage and requires RAD51 and RAD52, as well as the classical quelling factors QDE-1 and QDE-3 [58]. The second (disiRNA) pathway targets non-repetitive loci associated with sense/antisense transcription, does not involve QDE-1 and QDE-3 [35], but depends on the exonuclease ERI1 [34]. Our results set these processes apart from RIQ (which needs QDE-1 and QDE-3 but not RAD51, RAD52, or ERI1). Yet RIQ and canonical quelling share the requirement for DNA replication and the H3K56 acetyltransferase RTT109 (which is also linked to DNA replication) [38]. In the case of RIQ, replication can be required to generate nascent chromatin [59], which may be particularly prone to developing critical maturation defects in the presence of TetR-GFP or NIT-2. Such defects may then lead to the loss of nucleosomes and the onset of silencing. The fact that NIT-2 belongs to the GATA family of pioneering transcription factors, which can recognize their binding sites in the context of nucleosomes [60], further suggests that nascent, rather than mature, chromatin provides a particularly favorable environment for the remodeling-dependent silencing.

With respect to the requirement for SAD-6, several types of RIQ appear to exist. While RIQ of the *tetO* array induced by TetR-GFP is absolutely dependent on SAD-6, low levels of *tetO*-derived sRNAs are still observed without SAD-6 upon nitrogen starvation. Further, RIQ of AT-rich DNA is only partially dependent on SAD-6, and RIQ of the *lacO* array occurs normally without SAD-6, implying that SAD-6 can be replaced by another factor (altogether, the *N. crassa* genome encodes 24 ATPases with predicted chromatin-remodeling functions [61]). Nevertheless, all types of RIQ involve perturbed chromatin, require QDE-1, and occur without RAD51, the only RecA-like recombinase in *N. crassa* [61]. All types of RIQ must also rely on transcription to produce single-stranded RNA that can be used as a template for synthesizing double-stranded RNA. While QDE-1 was proposed to mediate this initial step in the biogenesis of qiRNAs [62], the nature of the DNA-dependent RNA polymerase at the basis of RIQ remains unknown.

In *Neurospora*, two peculiar populations of sRNAs were previously described: one population corresponds to subtelomeric sRNAs, the other comprises sRNAs expressed at low background levels throughout the genome [35]. Notably, we have found that the levels of background sRNAs were apparently increased in all conditions linked to replication and recombination defects. In a subset of these conditions (specifically, without RAD51, RAD52, or RTT109), the levels of subtelomeric sRNAs became elevated as well. Neither of these effects was associated with the loss of QDE-3, consistent with the fact that QDE-3 plays a redundant role in DNA repair [63].

Perturbed chromatin provides a general signal for the remodeling-dependent silencing

The role of ATP-dependent remodelers in heterochromatin (re)assembly has been well established, with some archetypal examples including (in addition to ATRX-DAXX) the nucleolar remodeling complex (NoRC) [64], the nucleosome remodeling and deacetylase (NuRD) complex [65], Snf2/Hdac-containing repressor complex (SHREC) [66], as well as the helicases SMARCAD1 [67], HELLS/LSH [68] and its plant counterpart DDM1 [69,70]. These factors make nucleosomes more accessible or replaced altogether to promote the incorporation of histone variants or modifications favoring heterochromatin. Our results suggest that the aberrant binding of transcription factors (or other non-histone proteins) leads to a state of perturbed chromatin that may constitute a particularly favorable substrate for the remodeling-dependent silencing. In this situation, the 'canonical' role of such proteins or their ability to initiate transcription are not as critical as their capacity to induce the state of perturbed chromatin. Curiously, the occurrence of diverse transcription factors at mammalian pericentromeric repeats was reported [50,56,57]. While some of those factors promote heterochromatin directly, by recruiting specific silencing activities or driving transcription of non-coding RNAs [56], others may do so indirectly, by perturbing chromatin that can act as a general signal for silencing. In budding yeast, the tight binding of LacI

and TetR repressors to their operator arrays was shown to trigger transcriptional silencing [30,31]. According to our data, such a process (i) can be induced by canonical transcription factors, (ii) requires active chromatin remodeling, and (iii) may initiate the expression of small RNAs to mediate post-transcriptional silencing.

How does SAD-6 recognize perturbed chromatin? Because SAD-6 controls RIQ of diverse loci (*i.e.*, the *tetO* array versus AT-rich DNA), it is unlikely to rely on sequence-specific signals or secondary structures that may recruit its orthologs in other situations [71]. On the other hand, SAD-6-dependent RIQ is associated with low nucleosome occupancy and high MNase sensitivity, suggesting that SAD-6 may favor nucleosome-free DNA. This propensity is shared by metazoan ATRX, which also localizes to nucleosome-depleted regions, including heavily transcribed genes [12], free proviral DNA [72], and R-loops [13]. In human cells, 87% of ATRX sites are present in open chromatin [73], and ATRX was also shown to interact with nucleic acids *in vitro* [74].

The genome of *N. crassa* contains a large number of relatively short nucleosome-depleted regions [75], which appear to escape silencing. This fact suggests that a threshold amount of nucleosome-free chromatin might be required. In general, such threshold-dependent mechanisms may be utilized to avoid the undesired activation of silencing. Accordingly, the streamlined genome of *N. crassa* (due to the absence of natural repeats, except rDNA) may be compatible with an unusually low threshold value (on the order of a few kilobase pairs). Taken together with the fact that *N. crassa* represents as established microbial model that sports all major epigenetic pathways (including constitutive heterochromatin, dynamic DNA methylation and fully functional RNAi), the operation of such a low threshold makes *N. crassa* an ideal system for discovering and characterizing *de novo* silencing mechanisms.

In this study, the state of perturbed chromatin was induced by the aberrant association of non-histone proteins with the *tetO* array. Yet an equivalent condition could be possibly attained by other means, for example, as the result of recombination-independent homologous pairing [76]. This idea is supported by the role of SAD-6 in MSUD, which relies on such pairing to identify mismatching loci [20,22]. Overall, the proposed remodeling-dependent mechanism may underlie a number of processes featuring the *de novo* initiation of transcriptional and post-transcriptional silencing.

DECLARATION OF INTERESTS

The authors declare no competing interest.

AUTHOR CONTRIBUTIONS

F.C. & E.G. proposed experiments; F.C., S.C.R., J.K., S.C., & E.G. performed experiments; E.G. performed

analysis and wrote the manuscript.

ACKNOWLEDGMENTS

This work was supported by Agence Nationale de la Recherche (ANR-10-LABX-0062, ANR-19-CE12-0002) and Institut Pasteur.

METHODS

Plasmids

All plasmids were made by standard molecular cloning techniques and confirmed by Sanger sequencing. The plasmid carrying the *lacO–tetO* construct (pFOC104A) was produced by inserting the NheI-XbaI fragment of pLAU43 [32] into pTSN6 [29] cut with XbaI. This plasmid was propagated in the presence of gentamicin and kanamycin [32] in *E. coli* DH10B cells. All standard gene-deletion plasmids included a marker that conferred resistance to nourseothricin (clonNAT). Maps of all plasmids used in this study are provided in SI Data File 1.

Manipulation of *Neurospora* strains

I. Strains

All *Neurospora* strains used in this study are listed in Table S2. Standard names of all genes analyzed in this study are provided in Table S1.

II. Growth Media

Vogel's Medium N containing 1.5% sucrose (VM medium) was used for normal vegetative growth. The same medium was used for nitrogen starvation, except that ammonium nitrate was omitted (VM-N medium). These media could be supplemented with tetracycline (100 µg/µl), blasticidin S (0.1 µg/µl, to increase expression of FLAG-SAD-6), and hydroxyurea (0.1M), if needed. Colonial growth was induced by plating macroconidia or ascospores on sorbose agar (1x Vogel's Medium N salts, 3% agar, 2% sorbose, 0.1% dextrose). Nourseothricin (Jena Bioscience, cat. no. AB-101L) was added to the final concentration of 50 µg/ml, if needed. For crossing, Synthetic Cross medium was used [77], containing 2% sucrose, 0.2 µg/ml biotin, and solidified with 2% agar. Crosses were setup on agar slants in glass culture tubes (20 x 200 mm). Ejected ascospores were collected in drops of water, induced by heat (60 ºC for 30 min), and plated on sorbose agar at appropriate dilutions.

III. Transformations

1-2 µg of linearized plasmid DNA (in 10 µl of 1M sorbitol) were mixed with 20 µl of pelleted macroconidia (also in 1M sorbitol), incubated on ice for 20 min, and electroporated using the following parameters: 1500 V, 600 Ω, 25 µF, 2 mm gap. Following electroporation, macroconidia were mixed with 1 ml of cold 1M sorbitol.

For plasmids targeting *his-3* or *csr-1+*, macroconidia were plated on sorbose agar immediately. For plasmids carrying the nourseothricin resistance gene, macroconidia were allowed to recover at room temperature for 4-5 hours prior to plating. For genotyping, genomic DNA was prepared as previously described [78], except that mycelia were fragilized by lyophilization. Integration events were interrogated by PCR. Homokaryotic strains were obtained from primary transformants by macroconidiation. The structure of the *lacO–tetO* reporter locus was checked by a set of 4 PCRs using Expand Long Template PCR System (Roche) and the following primer pairs: P1/P3, P2/P5, P4/P7, and P6/P8 (Table S3). The *tetO* locus was checked analogously, using primer pairs P1/P7 and P6/P8 (Table S3).

Assaying genetic stability of the arrays by multiplex PCR

Genomic DNA was extracted as described above. PCR master mixes contained two pairs of primers. One pair was specific for the *lacO* array (primers P2/P3) or the *tetO* array (primers P6/P7). Another pair was used as a positive control and was specific for *spo11+* (primers P9/P10). PCR products were resolved on 1.5% agarose gels and imaged using Gel Doc EZ (Bio-Rad).

Standard nitrogen starvation protocol

~10^6 macroconidia were inoculated into 150 ml of VM medium; cultures were grown in Erlenmeyer flasks at 30 ^{o}C for 24 hours, shaking at 180 rpm. Per each sample: mycelial mass was transferred into a chilled vacuum filtration unit, rinsed 5 times with 100 ml of chilled water, returned back to growth for 5 hours at 30 ^{o}C in 150 ml of VM-N medium, and then collected by filtration. Half of the mycelial mass was squeeze-dried, ground to fine powder in liquid nitrogen, and stored at -80 ^{o}C; the other half was crosslinked first (as described below).

Nitrogen starvation protocol including treatment(s) with 0.1M hydroxyurea (HU)

~10^6 macroconidia were inoculated into 130 ml of VM medium; cultures were grown in Erlenmeyer flasks at 30 ^{o}C for 19 hours, shaking at 180 rpm. Cultures were adjusted to 130 g (in fresh flasks), supplemented with 20 ml of VM medium containing 1.14 g of HU, and returned back to growth for additional 5 hours at 30 ^{o}C. Per each sample: mycelial mass was then transferred into a chilled vacuum filtration unit, rinsed 5 times with 100 ml of chilled water, and returned back to growth for 5 hours at 30 ^{o}C in 150 ml of pure VM-N medium or in 150 ml of VM-N medium with 0.1M HU. Samples were collected by filtration and processed as described in the standard protocol.

Chromatin immunoprecipitation (ChIP)

~10^6 macroconidia were inoculated into 150 ml of VM medium; cultures were grown in Erlenmeyer flasks at 30 ^{o}C for 24 hours, shaking at 180 rpm. If needed, cultures were supplemented with tetracycline (100 µg/µl)

or/and blasticidin (0.1 µg/µl). Mycelia were collected by filtration and washed with phosphate-buffered saline (PBS) at room temperature. Samples were squeezed-dried and transferred into 100 ml of PBS containing 1% formaldehyde. Typically, 1-2 g of squeeze-dried mycelial mass were obtained. Crosslinking proceeded for 30 min at room temperature, with constant stirring. After crosslinking was quenched with glycine, samples were collected by filtration, washed with PBS, squeeze-dried, ground to fine powder in liquid nitrogen, and stored at -80 ºC. The same sample was used for ChIP-seq and MNase-seq experiments.

For each sample, 150 mg of mycelial powder were combined with 1 ml of lysis buffer [140 mM NaCl; 1 mM EDTA; 1% Triton X-100; 0.1% sodium deoxycholate; 50 mM HEPES pH 7.5] containing 20 µl of proteinase inhibitors [Roche, cat. no. 11873580001, one tablet dissolved in 1 ml of PBS]. Samples were transferred into 15-ml TPX tubes and sonicated using Bioruptor Plus (Diagenode) with the following parameters: high power mode, 20 cycles, 90 sec ON & 90 sec OFF, 4 ºC. After sonication, samples were centrifuged twice for 5 min at 13000 ×g, 4 ºC. SureBeads Protein A Magnetic Beads (Bio-Rad) were used for all IPs. Concentrated beads were washed and diluted five-fold in lysis buffer. The protocol included the following steps. First, each ChIP sample was pre-cleared using 20 µl of diluted beads (4 hours at 4 ºC). Second, 25 µl of each pre-cleared ChIP sample were saved as 'Input'. Third, an appropriate antibody (0.5-1.0 µl) was added and allowed to recognize its targets overnight (at 4 ºC). The following antibodies were used: anti-FLAG (Sigma F1804), anti-H3K9me3 (Active Motif AB_2532132), anti-hH2B (Abcam ab1790), anti-hH3 (Abcam ab1791), and anti-GFP (Abcam ab290). Fourth, 20 µl of diluted beads, washed in lysis buffer containing 0.1% Tween-20, were added to each sample and incubated for 4 hours at 4 ºC (all incubations were done using a rotating wheel). Fifth, beads were washed in the following buffers (1 ml, for 10 min): {i} lysis buffer (twice), {ii} lysis buffer with 0.5M NaCl, {iii} wash buffer [250 mM LiCl; 0.5% IGEPAL; 0.5% sodium deoxycholate; 1 mM EDTA; 10 mM TrisHCl pH 8.0], and {iv} TE buffer [1 mM EDTA; 10 mM TrisHCl pH 8.0]. Elution was done using TES buffer [1% SDS; 10 mM EDTA; 50 mM TrisHCl pH 8.0], for 10 min at 65 °C. Input fractions were also treated with TES buffer in parallel. Fractions were decrosslinked at 65 °C overnight, treated with RNAse A and then Proteinase K. DNA was purified by phenol-chloroform extraction, precipitated with ethanol, resuspended in 20 µl of TE buffer, and quantified using the Qubit dsDNA HS assay kit (Invitrogen). Two separate cultures (representing independent biological replicates) were analyzed for each condition.

MNase sensitivity analysis

For each sample, 80 mg of crosslinked mycelial powder were combined with 1 ml of lysis buffer including 20 µl of proteinase inhibitors (prepared as described above) and 2 mM $CaCl_2$. Samples were mixed, equilibrated on ice for 10 min, mixed again, supplemented with 10 µl of MNase (NEB, cat. no. M0247S), and incubated in ThermoMixer C (Eppendorf) for 30 min at 37 ºC. Reactions were stopped by adding 30 µl of 0.5M EGTA pH

8.0. Samples were centrifuged twice for 10 min at 16000 ×g, 4 ºC. For decrosslinking, 50 µl of each sample were combined with 200 µl of TES buffer and incubated at 65 °C overnight, after which samples were treated with RNAse A and then Proteinase K. DNA was purified analogously to the ChIP protocol, and resuspended in 30 µl of TE buffer. DNA concentrations were measured using the Qubit dsDNA HS assay kit (Invitrogen).

Preparing ChIP-seq and MNase-seq libraries

ChIP-seq and MNase-seq libraries were made using the NEBNext Ultra II DNA Library Prep Kit for Illumina (NEB, cat. no. E7645S) and Agencourt Ampure XP beads (Beckman Coulter, cat. no. A63880), following the manufacturer's instructions. Depending on the amount of starting material, libraries were amplified with 10-11 cycles of PCR. All ChIP-seq and MNase-seq libraries created and analyzed in this study are listed in Table S4 and Table S5, respectively.

Isolating small RNAs

Total RNA was extracted from ground mycelia with TRI Reagent (Sigma-Aldrich) and dissolved in 5M urea. RNA with a RINe score above 9.5 (as determined by the 4150 TapeStation System) was fractionated on 8% TBE-Urea gels. Approximately 60 µg of RNA were loaded on each gel, distributed in 6 wells. Populations of small RNAs in the 17-26 nt range were excised as gel slices. The latter were crushed and incubated overnight in 0.3 M NaCl at 25 ºC, shaking at 850 rpm. All gel debris was removed using 0.22-µm spin columns (Sigma-Aldrich, cat. no. CLS8161). Small RNAs were precipitated by adding 4 volumes of ethanol and centrifuging for 40 min at 20000 ×g, 4 ºC. Pellets were dissolved in the total of 12 µl of water (per each gel). Two separate cultures (representing independent biological replicates) were analyzed for each condition.

Preparing sRNA-seq libraries

sRNA-seq libraries were made as previously described [20]. For each library, 5 µl of sRNA sample were used, corresponding to 25 µg of total RNA (however, because a fraction of sRNAs was lost during purification, the amount of total RNA corresponding to each sRNA sample should be less). All sRNA-seq libraries created and analyzed in this study are listed in Table S6.

Designing custom genome references

Basic custom meta-genome reference (*mNC12*) was created by concatenating the following GenBank entries: NC_026614.1, part of M54787.1 encoding the *mat a* locus (3237 bp), NC_026501.1, NC_026502.1, NC_026503.1, NC_026504.1, NC_026505.1, NC_026506.1, NC_026507.1, NW_011929459.1, NW_011929460.1, NW_011929461.1, NW_011929462.1, NW_011929463.1, NW_011929464.1, NW_011929465.1, NW_011929466.1, NW_011929467.1, NW_011929468.1, NW_011929469.1,

NW_011929470.1, NW_011929471.1. Genome references *mNC12.lacO-tetO* and *mNC12.tetO* (provided in SI Data File 2) were created by altering the sequence between *his-3* and *lpl* in *mNC12* to reflect the structure of the *his-3–lpl* locus in Strain A and Strain E, respectively.

Sequencing libraries

All libraries were analyzed on the Agilent 4150 TapeStation System using D5000 and D1000 ScreenTapes for ChIP-seq/MNase-seq and sRNA-seq samples, respectively. 48 libraries were combined and sequenced on the NextSeq 500 machine (Illumina) using the High Output Kit v2.5 (75 cycles, single-end mode). Typically, 460-500 million indexed reads were generated, corresponding to the average library size of 10 million reads. Raw sequencing data were demultiplexed using bcl2fastq (v2.20) with '--barcode-mismatches 0 --no-lane-splitting' flags. Adapter sequences were removed using cutadapt (v1.15) [79].

Sequence alignment and post-processing

All sequences were aligned to *mNC12.lacO-tetO* as the standard reference. In addition, sequences originating from Strain E and its derivatives were aligned to *mNC12.tetO*; while sequences derived from strains carrying parts of the *lacO* array were aligned to custom references reflecting the corresponding structure of the *his-3–lpl* locus. All alignments were done using bowtie2 (v2.3.4.1) with a standard set of parameters defined by the '--very-sensitive' option [80]. ChIP-seq/MNase-seq reads were aligned to the genome reference directly, while sRNA-seq reads were first aligned to the *mito_ribo* reference (provided in SI Data File 2), and the unaligned reads were retained and aligned to the genome reference. The alignments were post-processed using samtools (v1.7) [81].

Building and analyzing genomic profiles

For each library, a separate genome-wide profile was constructed by tabulating the number of reads mapped over a set of non-overlapping 500-bp tiles. Reads were counted with the command 'samtools view -c' based on the alignments to *mNC12.lacO-tetO*. Profiles were normalized by the effective number of reads. For ChIP-seq/MNase-seq samples, this value was equal to the total number of reads minus the number of mitochondrial reads. For sRNA-seq samples, both mitochondrial and ribosomal reads were subtracted. Profiles of biological replicates were averaged to produce the final profile used for analysis. High-resolution profiles were created by exactly the same approach, except that the tile size was 1 bp. For all logarithmic operations, profile values were augmented by 1. For plotting genome-wide maps of read-count ratios, profile values in the denominator were also augmented by 1. All graphs were generated using ggplot2 [82]. Euler diagrams were created using the eulerr R package (v7.0.0, https://CRAN.R-project.org/package=eulerr).

FIGURE LEGENDS

Figure 1. Constitutive heterochromatin and recombination-independent quelling (RIQ) are induced by the association of TetR-GFP with the *tetO* array.

(A) Group of isogenic strains created by a series of homologous transformations based on Strain O.

(B) Density of ChIP-seq reads over the *lacO–tetO* reporter and the neighboring genes (per 1 bp, per 1 million mapped reads). Unless noted otherwise, all profiles are plotted to the same scale, corresponding to the default scale bar in the upper right corner. The assayed region is 26000 bp long.

(C) Density of sRNA-seq reads, defined and plotted as in (B). The default scale bar is provided on the right.

(D) Properties of sRNAs expressed from the *tetO* array.

(E) Density of sRNA-seq reads in the 0.8-Mbp genomic region around the *lacO–tetO* locus (per 500 bp, per 1 million mapped reads). The absolute density (in Strain A) and the relative density (in Strain B, normalized by Strain A) are displayed in the lower and the upper panels, respectively.

(F) Changes in the levels of array-derived sRNAs, relative to Strain B and normalized by the levels of sRNAs expressed from the reference loci. Corresponding raw data are plotted in (G).

(G) Scatter plots showing genome-wide changes in sRNA expression. To enable log10-transformation without omitting any data, the number of reads (calculated per 500 bp, per 1 million mapped reads) was augmented by 1. The tiles covering the *lacO* array, the *tetO* array, and the reference loci are labeled by pink, green, and light blue circles, respectively. Populations of sRNAs over-expressed from subtelomeric regions and AT-rich DNA are marked by red and blue arrows, respectively.

Figure 2. Chromatin remodeler SAD-6 directly controls all silencing of the repressor-bound *tetO* array.

(A) Scatter plots showing genome-wide changes in sRNA expression (analyzed as in Fig. 1G).

(B) Density of ChIP-seq reads over the arrays and the neighboring genes (analyzed as in Fig. 1B).

(C) Scatter plots showing the relationship between MNase sensitivity and GC-content. The same set of 500-bp tiles was used as in (A). The tiles covering the *lacO* array (pink circles) and the *tetO* array (green circles) are indicated.

(D) Density of ChIP-seq reads over the arrays and the neighboring genes (analyzed as in (B)).

(E) Scatter plots showing the relationship between histone occupancy and GC-content. Strongly nucleosome-depleted regions (SNDRs) were defined by having the log10-transformed (IP[hH3]+1)/(Input+1) ratio less or equal to -0.5. The tiles covering the *lacO* array (pink circles) and the *tetO* array (green circles) are indicated.

(F) Density of ChIP-seq reads over the arrays and the neighboring genes (analyzed as in (B)).

Figure 3. Conserved GATA factor NIT-2 induces silencing of the *tetO* array analogously to TetR-GFP.

(A) Sequence comparison of the DNA binding domains of NIT-2 and the yeast GATA factor Gat1.

(B) Example of a gene strongly and directly regulated by NIT-2 [45]. Only a few of GATA motifs are found in promoters of such genes.

(C) Standard protocol for inducing acute nitrogen starvation.

(D) Densities of ChIP-seq and sRNA-seq reads over the *tetO* array and the neighboring genes (analyzed as in Fig. 1B,C). A short nucleosome-depleted region including the promoters of two divergently transcribed genes (one of which is *his-3*) is indicated with an asterisk. The assayed region is 26000 bp long.

(E) Scatter plots showing genome-wide changes in sRNA expression (analyzed as in Fig. 1G). The tiles that cover the *tetO* array (green circles) and the reference loci (light blue circles) are indicated.

(F) Density of ChIP-seq reads over the *tetO* array and the neighboring genes (analyzed as in (D)).

(G) Scatter plots showing the relationship between histone occupancy (after nitrogen starvation in the absence of SAD-6) and GC-content (analyzed as in Fig. 2E). The tiles covering the array are indicated (green circles).

(H) Histogram showing the relationship between SNDR length (defined as the number of consecutive 500-bp SNDR tiles) and abundance. The *tetO* array corresponds to a pair of exceptionally long SNDRs (containing 8 500-bp tiles each).

(I) Scatter plots showing the relationship between MNase sensitivity and GC-content (analyzed as in Fig. 2E).

Figure 4. Recombination-independent quelling induced by NIT-2 requires DNA replication.

(A) Modifications of the standard protocol (Fig. 3C) that incorporate treatments with 0.1M hydroxyurea (HU) before and (optionally) during starvation.

(B) Density of sRNA-seq reads over the *tetO* array and the neighboring genes (analyzed as in Fig. 3D).

(C) Scatter plot showing the relationship between changes in sRNA expression and GC-content. The tiles that cover the *tetO* array are indicated (green circles).

Figure 5. AT-rich DNA becomes subject to recombination-independent quelling modulated by SAD-6.

(A) Group of isogenic strains created by a series of homologous transformations based on Strain C (produced by a cross of Strain A with another strain carrying *dim-5Δ* and *set-7Δ*).

(B) Scatter plot showing the relationship between changes in sRNA expression versus GC-content (analyzed as in Fig. 4C). The tiles covering the *lacO* array (pink circles) and the *tetO* array (green circles) are indicated.

(C) Scatter plots showing the relationship between histone H3 occupancy and GC-content (analyzed as in Fig. 2E). The tiles covering the *lacO* array (pink circles) and the *tetO* array (green circles) are indicated.

(D) Scatter plots showing genome-wide changes in sRNA expression (analyzed as in Fig. 1G). A population of sRNAs affected differentially by the deletions of *qde-1+* and *sad-6+* is indicated (brown arrows). The tiles covering the reference loci are also indicated (light blue circles).

(E) Changes in sRNA expression across Chromosome I, represented by ratios of sRNA-seq reads (analyzed as

in Fig. 1E). The position of the centromere is indicated.

(F) Euler diagrams depicting the relationships among several groups of genomic loci (represented by the 500-bp tiles). AT-rich DNA tiles were defined by GC-content of 38% or less. Other thresholds corresponded to the five-fold change in sRNA expression (defined as ratios of sRNA-seq counts).

(G) Scatter plot showing the relationship between changes in sRNAs levels (analyzed as in (B)) and changes in chromatin accessibility to MNase under the indicated conditions. AT-rich DNA is defined as in (F).

Figure 6. Transcriptional and post-transcriptional silencing can be initiated by the active remodeling of a transiently nucleosome-depleted chromatin state.

Canonical nucleosome-rich organization of chromatin (designated as state N) can be perturbed by the aberrant association of non-histone proteins with DNA. This transition may be stimulated by DNA replication or other processes that promote nucleosome eviction or/and turnover. Perturbed chromatin organization (designated as state M) exhibits strong nucleosome depletion and high MNase sensitivity; yet, somewhat paradoxically, it is not competent for silencing. Instead, the silencing is initiated as the result of the active remodeling of state M back to state N (or a similar nucleosome-rich state N').

SUPPLEMENTARY INFORMATION (SI)

SI FIGURE LEGENDS

Figure S1. Properties of the experimental system.

(A) Schematic representation of the *lacO–tetO* reporter. The *lacO* and *tetO* arrays (originally provided on the plasmids pLAU43 and pLAU44 [32]) contained 168 *lacO1* and 191 *tetO* sites, and were characterized by GC-content of ~40% and ~50%, respectively. Three perfect repeats were also found in the *lacO* array. The arrays were combined on the plasmid pFOC104A and inserted by homologous recombination near the *his-3* gene of Strain O to create Strain A (Table S2).

(B) Examples of the reference sRNA-seq loci used to normalize and compare levels of array-derived sRNAs. Such loci exhibited strong and invariant patterns of expression, and they often comprised tRNA and 5S RNA genes. For the purpose of this analysis, these loci were represented by 463 500-bp tiles.

(C) Scatter plots showing genome-wide changes in sRNA expression (analyzed as in Fig. 1G). Reference loci are indicated (light blue circles). The expression of the reference loci remained concordant between different studies and experimental conditions.

(D) Histogram showing the composition of the *N. crassa* genome with respect to GC-content (analyzed using the same set of tiles as in Fig. 1G). The fraction of AT-rich DNA (characterized by GC-content of 38% or less) can be clearly identified.

Figure S2. Silencing of the repressor-bound *tetO* array: properties and regulation (Part I).

(A) Densities of ChIP-seq and sRNA-seq reads over the arrays and the neighboring genes (analyzed as in Fig. 1B,C).

(B) Density of ChIP-seq reads over the arrays and the neighboring genes (analyzed as in (A)).

(C) Scatter plots showing the relationship between histone H3 occupancy and GC-content (analyzed as in Fig. 2E). The tiles covering the *lacO* array (pink circles) and the *tetO* array (green circles) are indicated.

(D) Scatter plots showing the relationship between changes in histone H3 occupancy versus GC-content. The tiles covering the *lacO* array (pink circles) and the *tetO* array (green circles) are indicated.

Figure S3. Silencing of the repressor-bound *tetO* array: properties and regulation (Part II).

(A) Scatter plots showing the relationship between changes in sRNA expression and GC-content (analyzed as in Fig. 4C). The tiles covering the *lacO* array (pink circles) and the *tetO* array (green circles) are indicated.

(B) Density of sRNA-seq reads over the arrays and the neighboring genes (analyzed as in Fig. 1C). The increased expression of background sRNAs is evidenced by having multiple reads mapped to *his-3* and *lpl*.

(C) Changes in sRNA expression across the genome (analyzed as in Fig. 1E).

Figure S4. Chromatin remodeler CHD1 is not required for silencing of the repressor-bound *tetO* array.

(A) Density of ChIP-seq reads over the arrays and the neighboring genes (analyzed as in Fig. 1B).

(B) Scatter plots showing genome-wide changes in sRNA expression (analyzed as in Fig. 1G).

(C) Scatter plot showing the relationship between histone H3 occupancy and GC-content (analyzed as in Fig. 2E).

(D) Scatter plots showing the relationship between changes in histone H3 occupancy and H3K9me3 versus GC-content (analyzed as in Fig. S2D).

Figure S5. SAD-6 may have additional chromatin-centered roles in *N. crassa*.

(A) Density of sRNA-seq reads over the arrays and the neighboring genes (analyzed as in Fig. 1C).

(B) Scatter plots showing the relationship between changes in histone occupancy and H3K9me3 versus GC-content (analyzed as in Fig. S2D). The tiles covering the *lacO* array (pink circles) and the *tetO* array (green circles) are indicated.

(C) Scatter plots showing the relationship between changes in MNase sensitivity versus GC-content. The tiles covering the *lacO* array (pink circles) and the *tetO* array (green circles) are indicated.

(D) Histogram showing the relationship between SNDR length (defined as the number of consecutive 500-bp SNDR tiles) and abundance. The *tetO* array corresponds to a pair of exceptionally long SNDRs (containing 8 500-bp tiles each).

(E) Schematic of a construct (provided on the plasmid pFOC109N) that was used to create a strain expressing FLAG-tagged SAD-6 protein ('Strain B: *flag-sad-6*').

(F) Changes in sRNA expression across the genome (analyzed as in Fig. 1E).

(G) Changes in histone H3 occupancy & H3K9me3 across the genome, calculated as ratios of ChIP-seq reads.

(H) Changes in MNase sensitivity across the genome, calculated as ratios of ChIP-seq reads.

(I) Changes in FLAG-SAD-6 occupancy across the genome, calculated as ratios of ChIP-seq reads.

(J) Region *r1*, in which the expression sRNAs is strongly downregulated in the absence of SAD-6.

(K) Region *r2*, in which constitutive heterochromatin is nearly eliminated in the absence of SAD-6.

(L) Region *r3*, characterized by strong enrichment in FLAG-SAD-6.

Figure S6. Starvation-induced silencing: properties and regulation.

(A) Densities of ChIP-seq and sRNA-seq reads over the *tetO* array and the neighboring genes (analyzed as in Fig. 3D).

(B) Changes in sRNA expression across the genome (analyzed as in Fig. 1E).

(C) Changes in histone H3 occupancy & H3K9me3 across the genome (analyzed as in Fig. S5G).

(D) Changes in MNase sensitivity across the genome (analyzed as in Fig. S5H).

Figure S7. Properties of recombination-independent quelling of the *lacO* array and AT-rich DNA

(A) Densities of ChIP-seq and sRNA-seq reads over the arrays and the neighboring genes (analyzed as in Fig. 1B,C).

(B) Scatter plots showing genome-wide changes in sRNA expression (analyzed as in Fig. 1G). The tiles that cover the *lacO* array (pink circles) and the *tetO* array (green circles) are indicated.

(C) Scatter plot showing the relationship between changes in sRNA expression and GC-content (analyzed as in Fig. 4C). The tiles covering the *lacO* array (pink circles) and the *tetO* array (green circles) are indicated.

(D) Densities of ChIP-seq and sRNA-seq reads over the arrays and the neighboring genes (as in (A)).

(E) Scatter plot showing the relationship between changes in sRNA expression and GC-content (analyzed as in (C)). The tiles covering the *lacO* array (pink circles) and the *tetO* array (green circles) are indicated.

(F) Scatter plots showing the relationship between hH3 occupancy and GC-content (analyzed as in Fig. 2E). The tiles covering the *lacO* array (pink circles) and the *tetO* array (green circles) are indicated.

(G) Scatter plots showing the relationship between MNase sensitivity and GC-content (analyzed as in Fig. 2C).

(H) Density of sRNA-seq reads over the arrays and the neighboring genes (analyzed as in (A)). The *lacO* array in 'Strain B: *sad-6Δ*' was found to contain a large deletion.

Figure S8. Assaying genetic stability of the *lacO* and *tetO* arrays.

(A) Strategy to generate a clonal population of nuclei, in which the stability of the arrays was assayed. Several macroconidial isolates from a primary vegetative culture were tested by multiplex PCR for the presence of the arrays. A single primary clone with the confirmed arrays was chosen to start a secondary culture, from which 28 random progeny were selected and re-assayed for the presence of the arrays.

(B) PCR products were resolved on agarose gels. Missing products (corresponding to deletions) are indicated by red rectangles.

Figure S9. Heterochromatin assembly and recombination-independent quelling of the *lacO* array can be decoupled.

(A) Strategy to create a group of isogenic strains carrying deletions in the *lacO* array.

(B) Density of sRNA-seq reads over the arrays and the neighboring genes (analyzed as in Fig. 1C).

(C) Density of ChIP-seq reads over the arrays and the neighboring genes (analyzed as in Fig. 1B).

(D) Strategy to create a group of isogenic strains carrying fragments of the *lacO* array.

(E) Deletions and insertions of the *lacO* array analyzed in this study.

(F) Density of sRNA-seq reads over the *lacO* fragment and the neighboring genes (analyzed as in (B)).

(G) Density of ChIP-seq reads over the *lacO* fragment and the neighboring genes (analyzed as in (C)).

SI TABLES

Table S1. *Neurospora* genes analyzed in this study.

Table S2. *Neurospora* strains used in this study.

Table S3. Diagnostic primers used in this study.

Table S4. ChIP-seq libraries created and analyzed in this study.

Table S5. MNase-seq libraries created and analyzed in this study.

Table S6. sRNA-seq libraries created and analyzed in this study.

In Tables S4-S6, the following notations of the culturing conditions were used:

'Tc' - growing cultures were supplemented with 100 μg/μl of tetracycline;

'Bl' - growing cultures were supplemented with 0.1 μg/μl of blasticidin S;

'HU' - pre-grown cultures were incubated for 24 hours in the standard medium supplemented with 0.1M HU;

'no-N' - cultures were shifted to the nitrogen-free medium without HU block;

'N+ control' - cultures were processed analogously to 'no-N' but shifted to the standard (N+) medium instead;

"maintained" - cultures were treated with HU and shifted to the nitrogen-free medium containing HU;

"released" - cultures were treated with HU and shifted to the nitrogen-free medium without HU.

SI DATA FILES

Available at https://figshare.com/s/68987d7763146c2a4e2c; DOI: 10.6084/m9.figshare.24943173

Data File 1. Maps of plasmids used in this study.

Provided as plain-text files in EMBL format, compressed with TAR/GZIP.

Data File 2. Custom genome references used in this study.

Provided as plain-text files in EMBL format, compressed with TAR/GZIP. The following genome references are included: *mNC12.lacO-tetO*, *mNC12.tetO*, and *mito_ribo*.

Data File 3. 500-bp tiles representing reference sRNA-seq loci.

Provided as a plain-text file in CSV format, compressed with TAR/GZIP. Tile coordinates correspond to the genome reference *mNC12.lacO-tetO*.

REFERENCES

1. Almeida, M.V. *et al.* (2022) Taming transposable elements in vertebrates: from epigenetic silencing to domestication. *Trends Genet* 38, 529–553
2. Allshire, R.C. and Madhani, H.D. (2018) Ten principles of heterochromatin formation and function. *Nat Rev Mol Cell Biol* 19, 229–244
3. Janssen, A. *et al.* (2018) Heterochromatin: Guardian of the Genome. *Annu. Rev. Cell Dev. Biol.* 34, 265–288
4. Hamel, J. and Tawil, R. (2018) Facioscapulohumeral Muscular Dystrophy: Update on Pathogenesis and Future Treatments. *Neurotherapeutics* 15, 863–871
5. Bull, J.H. and Wootton, J.C. (1984) Heavily methylated amplified DNA in transformants of Neurospora crassa. *Nature* 310, 701–704
6. Ye, F. and Signer, E.R. (1996) RIGS (repeat-induced gene silencing) in Arabidopsis is transcriptional and alters chromatin configuration. *Proc Natl Acad Sci U S A* 93, 10881–10886
7. Dorer, D.R. and Henikoff, S. (1994) Expansions of transgene repeats cause heterochromatin formation and gene silencing in Drosophila. *Cell* 77, 993–1002
8. Garrick, D. *et al.* (1998) Repeat-induced gene silencing in mammals. *Nature Genetics* 18, 56–59
9. Blewitt, M.E. *et al.* (2005) An N-ethyl-N-nitrosourea screen for genes involved in variegation in the mouse. *Proc Natl Acad Sci U S A* 102, 7629–7634
10. Daxinger, L. *et al.* (2013) An ENU mutagenesis screen identifies novel and known genes involved in

epigenetic processes in the mouse. *Genome Biol* 14, R96

11. Aguilera, P. and López-Contreras, A.J. (2023) ATRX, a guardian of chromatin. *Trends in Genetics* 39, 505–519
12. Schneiderman, J.I. *et al.* (2012) Nucleosome-depleted chromatin gaps recruit assembly factors for the H3.3 histone variant. *Proc Natl Acad Sci U S A* 109, 19721–19726
13. Nguyen, D.T. *et al.* (2017) The chromatin remodelling factor ATRX suppresses R-loops in transcribed telomeric repeats. *EMBO Rep* 18, 914–928
14. Selker, E.U. (1990) Premeiotic instability of repeated sequences in Neurospora crassa. *Annu. Rev. Genet.* 24, 579–613
15. Gladyshev, E. (2017) Repeat-Induced Point Mutation and Other Genome Defense Mechanisms in Fungi. *Microbiol Spectr* 5, 5.4.02
16. Gladyshev, E. and Kleckner, N. (2017) DNA sequence homology induces cytosine-to-thymine mutation by a heterochromatin-related pathway in Neurospora. *Nat Genet* 49, 887–894
17. Romano, N. and Macino, G. (1992) Quelling: transient inactivation of gene expression in Neurospora crassa by transformation with homologous sequences. *Mol Microbiol* 6, 3343–3353
18. Shiu, P.K.T. *et al.* (2001) Meiotic silencing by unpaired DNA. *Cell* 107, 905–916
19. Hammond, T.M. (2017) Sixteen years of meiotic silencing by unpaired DNA. *Ndv. Genet.* 97, 1–42
20. Rhoades, N. *et al.* (2021) Recombination-independent recognition of DNA homology for meiotic silencing in Neurospora crassa. *Proceedings of the National Academy of Sciences* 118, e2108664118
21. Zhang, Z. *et al.* (2013) Homologous recombination as a mechanism to recognize repetitive DNA sequences in an RNAi pathway. *Genes Dev* 27, 145–150
22. Samarajeewa, D.A. *et al.* (2014) Efficient detection of unpaired DNA requires a member of the rad54-like family of homologous recombination proteins. *Genetics* 198, 895–904
23. Aramayo, R. and Selker, E.U. (2013) Neurospora crassa, a model system for epigenetics research. *Cold Spring Harb Perspect Biol* 5, a017921
24. Smith, K.M. *et al.* (2010) H2B- and H3-specific histone deacetylases are required for DNA methylation in Neurospora crassa. *Genetics* 186, 1207–1216
25. Klocko, A.D. *et al.* (2019) Nucleosome Positioning by an Evolutionarily Conserved Chromatin Remodeler Prevents Aberrant DNA Methylation in Neurospora. *Genetics* 211, 563–578
26. Belden, W.J. *et al.* (2011) CHD1 remodels chromatin and influences transient DNA methylation at the clock gene frequency. *PLoS Genet* 7, e1002166
27. Dang, Y. *et al.* (2013) Convergent transcription induces dynamic DNA methylation at disiRNA loci. *PLoS Genet* 9, e1003761
28. Ruesch, C.E. *et al.* (2014) The histone H3 lysine 9 methyltransferase DIM-5 modifies chromatin at

frequency and represses light-activated gene expression. *G3 (Bethesda)* 5, 93–101

29. Nguyen, T.-S. and Gladyshev, E. (2020) Developing a tetO/TetR system in Neurospora crassa. *Fungal Genet Biol* 136, 103316
30. Loïodice, I. *et al.* (2021) An Inducible System for Silencing Establishment Reveals a Stepwise Mechanism in Which Anchoring at the Nuclear Periphery Precedes Heterochromatin Formation. *Cells* 10, 2810
31. Dubarry, M. *et al.* (2011) Tight protein-DNA interactions favor gene silencing. *Genes Dev* 25, 1365–1370
32. Lau, I.F. *et al.* (2003) Spatial and temporal organization of replicating Escherichia coli chromosomes. *Mol Microbiol* 49, 731–743
33. Forrest, E.C. *et al.* (2004) The RNA-dependent RNA polymerase, QDE-1, is a rate-limiting factor in post-transcriptional gene silencing in Neurospora crassa. *Nucleic Acids Res* 32, 2123–2128
34. Dang, Y. *et al.* (2016) Antisense transcription licenses nascent transcripts to mediate transcriptional gene silencing. *Genes Dev* 30, 2417–2432
35. Lee, H.-C. *et al.* (2010) Diverse pathways generate microRNA-like RNAs and Dicer-independent small interfering RNAs in fungi. *Mol Cell* 38, 803–814
36. Symington, L.S. *et al.* (2014) Mechanisms and regulation of mitotic recombination in Saccharomyces cerevisiae. *Genetics* 198, 795–835
37. Zhang, Z. *et al.* (2014) Histone H3K56 acetylation is required for quelling-induced small RNA production through its role in homologous recombination. *J Biol Chem* 289, 9365–9371
38. Dahlin, J.L. *et al.* (2015) Histone-modifying enzymes, histone modifications and histone chaperones in nucleosome assembly: Lessons learned from Rtt109 histone acetyltransferases. *Crit Rev Biochem Mol Biol* 50, 31–53
39. Freitag, M. *et al.* (2004) DNA methylation is independent of RNA interference in Neurospora. *Science* 304, 1939
40. Chicas, A. *et al.* (2005) Small interfering RNAs that trigger posttranscriptional gene silencing are not required for the histone H3 Lys9 methylation necessary for transgenic tandem repeat stabilization in Neurospora crassa. *Mol Cell Biol* 25, 3793–3801
41. Lu, M. and He, X. (2019) Intricate regulation on epigenetic stability of the subtelomeric heterochromatin and the centromeric chromatin in fission yeast. *Curr Genet* 65, 381–386
42. Basenko, E.Y. *et al.* (2015) Genome-wide redistribution of H3K27me3 is linked to genotoxic stress and defective growth. *Proc Natl Acad Sci U S A* 112, E6339-6348
43. Gould, D.J. and Chernajovsky, Y. (2004) Endogenous GATA factors bind the core sequence of the tetO and influence gene regulation with the tetracycline system. *Mol Ther* 10, 127–138
44. Fu, Y.H. and Marzluf, G.A. (1990) nit-2, the major positive-acting nitrogen regulatory gene of

Neurospora crassa, encodes a sequence-specific DNA-binding protein. *Proc Natl Acad Sci U S A* 87, 5331–5335

45. Huberman, L.B. *et al.* (2021) DNA affinity purification sequencing and transcriptional profiling reveal new aspects of nitrogen regulation in a filamentous fungus. *Proc Natl Acad Sci U S A* 118, e2009501118
46. Nolan, T. *et al.* (2008) The RNA-dependent RNA polymerase essential for post-transcriptional gene silencing in Neurospora crassa interacts with replication protein A. *Nucleic Acids Res* 36, 532–538
47. Sachs, M.S. *et al.* (1997) Expression of herpes virus thymidine kinase in Neurospora crassa. *Nucleic Acids Res* 25, 2389–2395
48. Jamieson, K. *et al.* (2016) Loss of HP1 causes depletion of H3K27me3 from facultative heterochromatin and gain of H3K27me2 at constitutive heterochromatin. *Genome Res* 26, 97–107
49. Holoch, D. and Moazed, D. (2015) RNA-mediated epigenetic regulation of gene expression. *Nat Rev Genet* 16, 71–84
50. Saksouk, N. *et al.* (2015) Constitutive heterochromatin formation and transcription in mammals. *Epigenetics & Chromatin* 8, 1600–1614
51. Zhou, J. *et al.* (2023) DDM1-mediated R-loop resolution and H2A.Z exclusion facilitates heterochromatin formation in Arabidopsis. *Sci Adv* 9, eadg2699
52. Skourti-Stathaki, K. *et al.* (2014) R-loops induce repressive chromatin marks over mammalian gene terminators. *Nature* 516, 436–439
53. Carlier, F. *et al.* (2021) Modulation of C-to-T mutation by recombination-independent pairing of closely positioned DNA repeats. *Biophysical Journal* 120, 4325–4336
54. Herbert, A. (2020) ALU non-B-DNA conformations, flipons, binary codes and evolution. *R. Soc. open sci.* 7, 200222
55. Wang, G. and Vasquez, K.M. (2023) Dynamic alternative DNA structures in biology and disease. *Nat Rev Genet* 24, 211–234
56. Saksouk, N. *et al.* (2014) Redundant mechanisms to form silent chromatin at pericentromeric regions rely on BEND3 and DNA methylation. *Mol Cell* 56, 580–594
57. Bulut-Karslioglu, A. *et al.* (2012) A transcription factor-based mechanism for mouse heterochromatin formation. *Nat Struct Mol Biol* 19, 1023–1030
58. Dang, Y. *et al.* (2014) Small RNA-Mediated Gene Silencing in Neurospora. In *Fungal RNA Biology* (Sesma, A. and Von Der Haar, T., eds), pp. 269–289, Springer International Publishing
59. MacAlpine, D.M. and Almouzni, G. (2013) Chromatin and DNA replication. *Cold Spring Harb Perspect Biol* 5, a010207
60. Zaret, K.S. and Carroll, J.S. (2011) Pioneer transcription factors: establishing competence for gene expression. *Genes Dev* 25, 2227–2241

61. Borkovich, K.A. *et al.* (2004) Lessons from the genome sequence of Neurospora crassa: tracing the path from genomic blueprint to multicellular organism. *Microbiol Mol Biol Rev* 68, 1–108
62. Lee, H.-C. *et al.* (2009) qiRNA is a new type of small interfering RNA induced by DNA damage. *Nature* 459, 274–277
63. Kato, A. and Inoue, H. (2006) Growth defect and mutator phenotypes of RecQ-deficient Neurospora crassa mutants separately result from homologous recombination and nonhomologous end joining during repair of DNA double-strand breaks. *Genetics* 172, 113–125
64. Postepska-Igielska, A. *et al.* (2013) The chromatin remodelling complex NoRC safeguards genome stability by heterochromatin formation at telomeres and centromeres. *EMBO Rep* 14, 704–710
65. Helbling Chadwick, L. *et al.* (2009) The Mi-2/NuRD complex associates with pericentromeric heterochromatin during S phase in rapidly proliferating lymphoid cells. *Chromosoma* 118, 445–457
66. Sugiyama, T. *et al.* (2007) SHREC, an Effector Complex for Heterochromatic Transcriptional Silencing. *Cell* 128, 491–504
67. Rowbotham, S.P. *et al.* (2011) Maintenance of silent chromatin through replication requires SWI/SNF-like chromatin remodeler SMARCAD1. *Mol Cell* 42, 285–296
68. Yu, W. *et al.* (2014) Genome-wide DNA methylation patterns in LSH mutant reveals de-repression of repeat elements and redundant epigenetic silencing pathways. *Genome Res* 24, 1613–1623
69. Osakabe, A. *et al.* (2021) The chromatin remodeler DDM1 prevents transposon mobility through deposition of histone variant H2A.W. *Nat Cell Biol* 23, 391–400
70. Lee, S.C. *et al.* (2023) Chromatin remodeling of histone H3 variants by DDM1 underlies epigenetic inheritance of DNA methylation. *Cell* 186, 4100-4116.e15
71. Teng, Y.-C. *et al.* (2021) ATRX promotes heterochromatin formation to protect cells from G-quadruplex DNA-mediated stress. *Nat Commun* 12, 3887
72. Lukashchuk, V. *et al.* (2008) Human cytomegalovirus protein pp71 displaces the chromatin-associated factor ATRX from nuclear domain 10 at early stages of infection. *J Virol* 82, 12543–12554
73. Truch, J. *et al.* (2022) The chromatin remodeller ATRX facilitates diverse nuclear processes, in a stochastic manner, in both heterochromatin and euchromatin. *Nat Commun* 13, 3485
74. Sarma, K. *et al.* (2014) ATRX directs binding of PRC2 to Xist RNA and Polycomb targets. *Cell* 159, 869–883
75. Ferraro, A.R. *et al.* (2021) Chromatin accessibility profiling in Neurospora crassa reveals molecular features associated with accessible and inaccessible chromatin. *BMC Genomics* 22, 459
76. Mazur, A.K. and Gladyshev, E. (2023) C-DNA may facilitate homologous DNA pairing. *Trends Genet* 39, 575–585
77. Westergaard, M. and Mitchell, H.K. (1947) Neurospora. V. A synthetic medium favoring sexual

reproduction. *American J of Botany* 34, 573–577

78. Gladyshev, E. and Kleckner, N. (2014) Direct recognition of homology between double helices of DNA in Neurospora crassa. *Nat Commun* 5, 3509
79. Martin, M. (2011) Cutadapt removes adapter sequences from high-throughput sequencing reads. *EMBnet j.* 17, 10
80. Langmead, B. and Salzberg, S.L. (2012) Fast gapped-read alignment with Bowtie 2. *Nat Methods* 9, 357–359
81. Danecek, P. *et al*. (2021) Twelve years of SAMtools and BCFtools. *Gigascience* 10, giab008
82. Wickham, H. (2016) *ggplot2: Elegant Graphics for Data Analysis*, Springer-Verlag New York

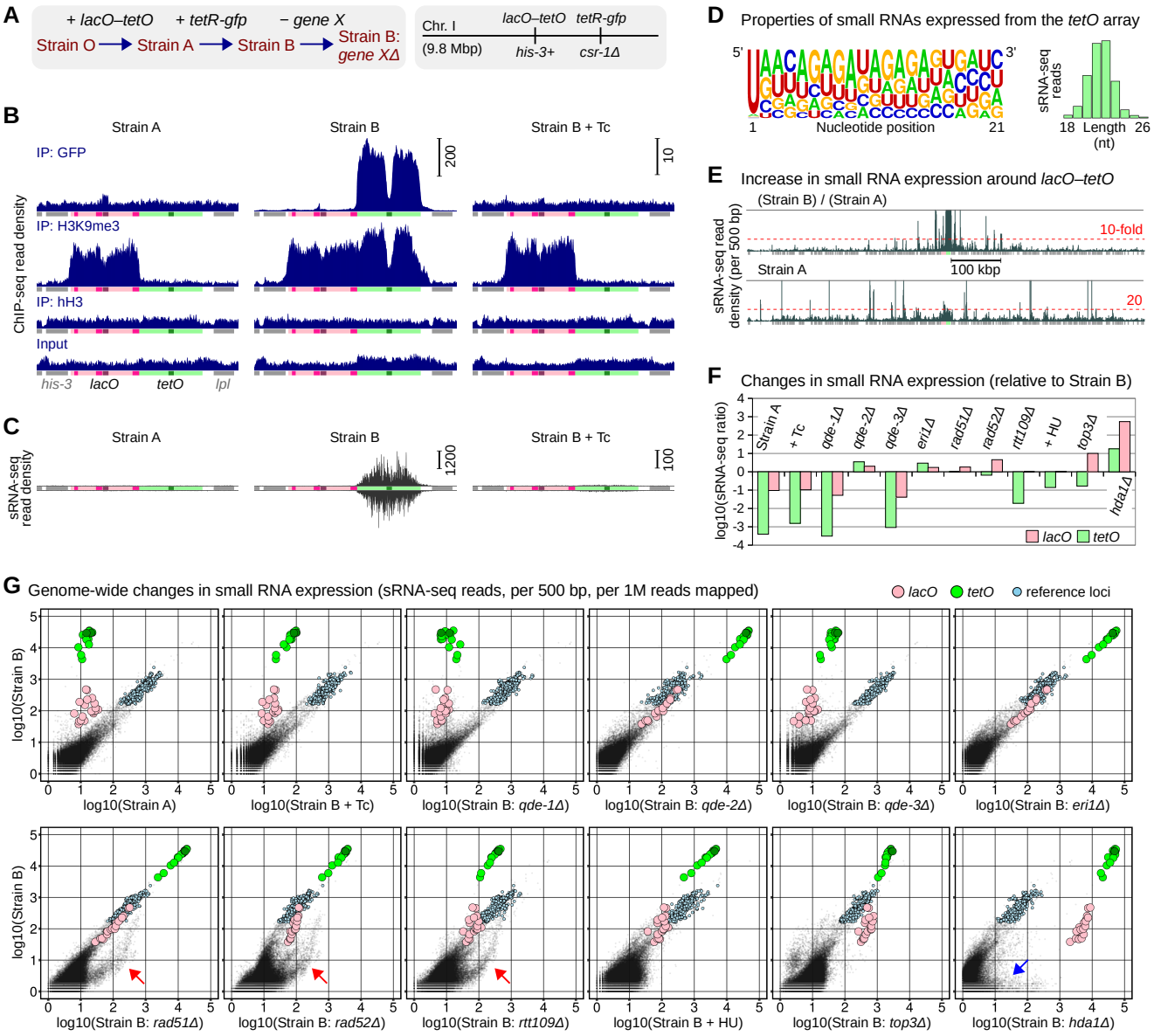
A
+ lacO–tetO
+ tetR-gfp
− gene X
Strain O
Strain A
Strain B
Strain B: gene XΔ
Chr. I
(9.8 Mbp)
lacO–tetO
tetR-gfp
his-3+
csr-1Δ
B
Strain A
Strain B
Strain B + Tc
IP: GFP
IP: H3K9me3
IP: hH3
Input
ChIP-seq read density
his-3
lacO
tetO
lpl
C
sRNA-seq read density
D
Properties of small RNAs expressed from the tetO array
Nucleotide position
sRNA-seq reads
Length (nt)
E
Increase in small RNA expression around lacO–tetO
(Strain B) / (Strain A)
10-fold
Strain A
100 kbp
20
sRNA-seq read density (per 500 bp)
F
Changes in small RNA expression (relative to Strain B)
log10(sRNA-seq ratio)
Strain A
+ Tc
qde-1Δ
qde-2Δ
qde-3Δ
eri1Δ
rad51Δ
rad52Δ
rtt109Δ
+ HU
top3Δ
hda1Δ
lacO
tetO
G
Genome-wide changes in small RNA expression (sRNA-seq reads, per 500 bp, per 1M reads mapped)
lacO
tetO
reference loci
log10(Strain B)
log10(Strain A)
log10(Strain B + Tc)
log10(Strain B: qde-1Δ)
log10(Strain B: qde-2Δ)
log10(Strain B: qde-3Δ)
log10(Strain B: eri1Δ)
log10(Strain B: rad51Δ)
log10(Strain B: rad52Δ)
log10(Strain B: rtt109Δ)
log10(Strain B + HU)
log10(Strain B: top3Δ)
log10(Strain B: hda1Δ)

Figure 1

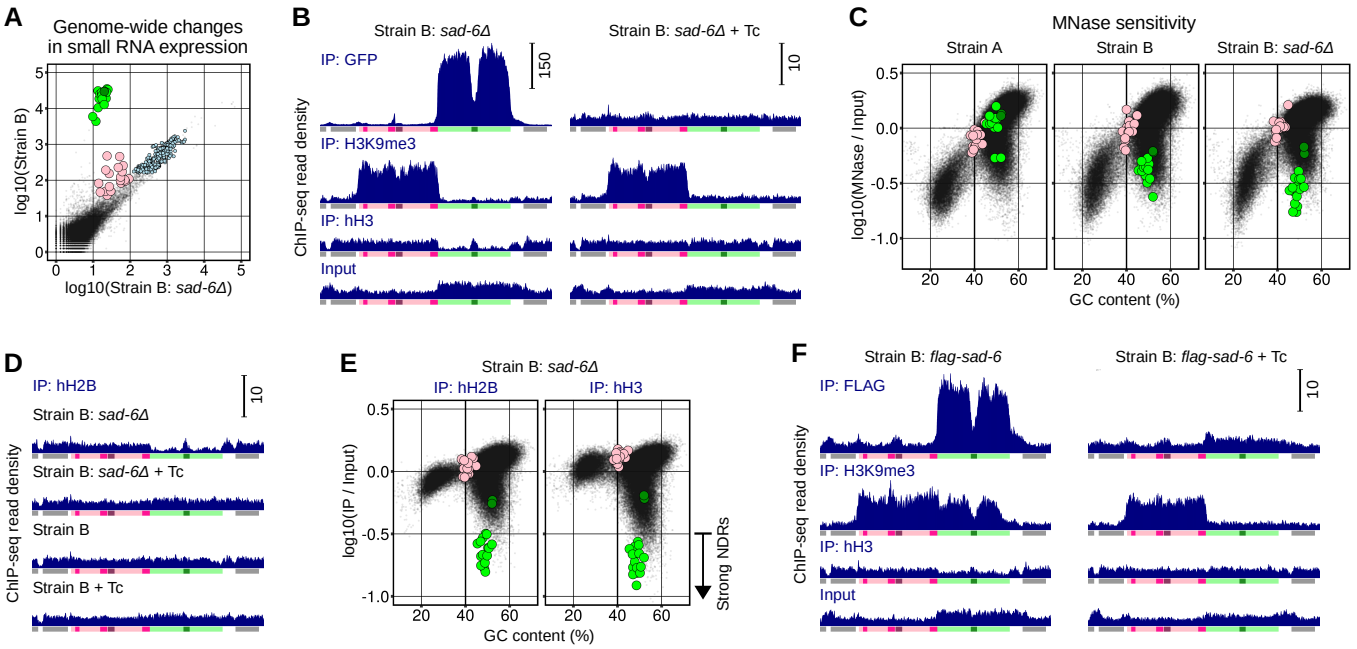
A
Genome-wide changes in small RNA expression
log10(Strain B)
log10(Strain B: sad-6Δ)
B
Strain B: sad-6Δ
Strain B: sad-6Δ + Tc
IP: GFP
IP: H3K9me3
IP: hH3
Input
ChIP-seq read density
150
10
C
MNase sensitivity
Strain A
Strain B
Strain B: sad-6Δ
log10(MNase / Input)
GC content (%)
D
IP: hH2B
Strain B: sad-6Δ
Strain B: sad-6Δ + Tc
Strain B
Strain B + Tc
ChIP-seq read density
10
E
Strain B: sad-6Δ
IP: hH2B
IP: hH3
log10(IP / Input)
GC content (%)
Strong NDRs
F
Strain B: flag-sad-6
Strain B: flag-sad-6 + Tc
IP: FLAG
IP: H3K9me3
IP: hH3
Input
ChIP-seq read density
10

Figure 2

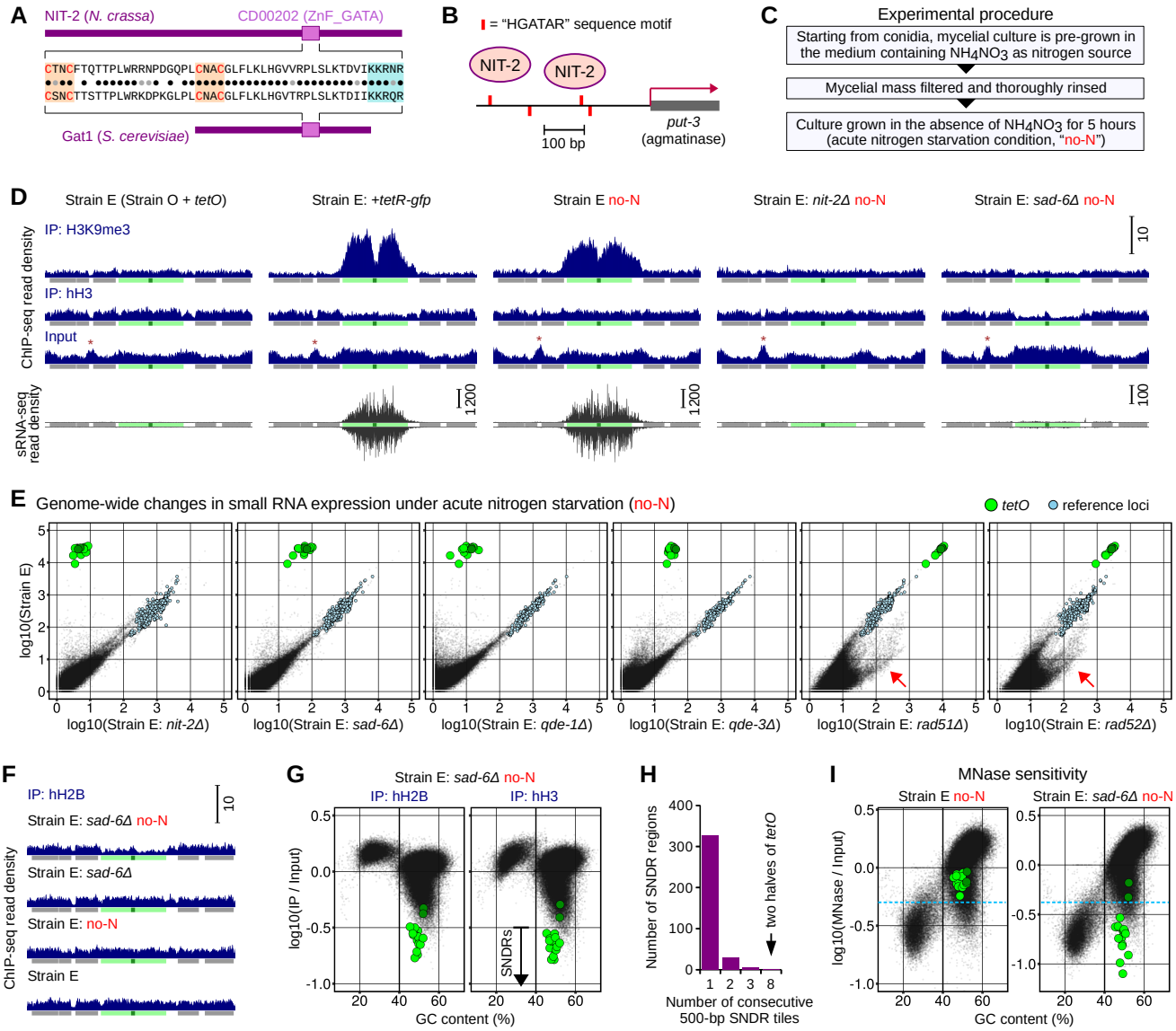
A
NIT-2 (N. crassa)
CD00202 (ZnF_GATA)
CTNCFTQTTPLWRRNPDGQPLCNACGLFLKLHGVVRPLSLKTDVIKKRNR
CSNCTTSTTPLWRKDPKGLPLCNACGLFLKLHGVTRPLSLKTDIIKKRQR
Gat1 (S. cerevisiae)
B
= "HGATAR" sequence motif
NIT-2
NIT-2
100 bp
put-3
(agmatinase)
C
Experimental procedure
Starting from conidia, mycelial culture is pre-grown in the medium containing NH4NO3 as nitrogen source
Mycelial mass filtered and thoroughly rinsed
Culture grown in the absence of NH4NO3 for 5 hours (acute nitrogen starvation condition, "no-N")
D
Strain E (Strain O + tetO)
Strain E: +tetR-gfp
Strain E no-N
Strain E: nit-2Δ no-N
Strain E: sad-6Δ no-N
IP: H3K9me3
IP: hH3
Input
ChIP-seq read density
sRNA-seq read density
10
1200
1200
100
E
Genome-wide changes in small RNA expression under acute nitrogen starvation (no-N)
tetO
reference loci
log10(Strain E)
log10(Strain E: nit-2Δ)
log10(Strain E: sad-6Δ)
log10(Strain E: qde-1Δ)
log10(Strain E: qde-3Δ)
log10(Strain E: rad51Δ)
log10(Strain E: rad52Δ)
F
IP: hH2B
Strain E: sad-6Δ no-N
Strain E: sad-6Δ
Strain E: no-N
Strain E
ChIP-seq read density
10
G
Strain E: sad-6Δ no-N
IP: hH2B
IP: hH3
log10(IP / Input)
SNDRs
GC content (%)
H
Number of SNDR regions
two halves of tetO
Number of consecutive 500-bp SNDR tiles
I
MNase sensitivity
Strain E no-N
Strain E: sad-6Δ no-N
log10(MNase / Input)
GC content (%)

Figure 3

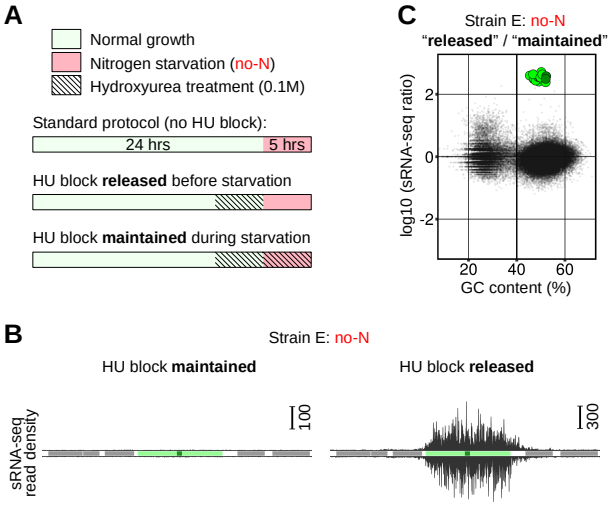
A
Normal growth
Nitrogen starvation (no-N)
Hydroxyurea treatment (0.1M)
Standard protocol (no HU block):
24 hrs
5 hrs
HU block released before starvation
HU block maintained during starvation
C
Strain E: no-N
"released" / "maintained"
log10 (sRNA-seq ratio)
2
0
-2
20
40
60
GC content (%)
B
Strain E: no-N
HU block maintained
HU block released
sRNA-seq read density
100
300

Figure 4

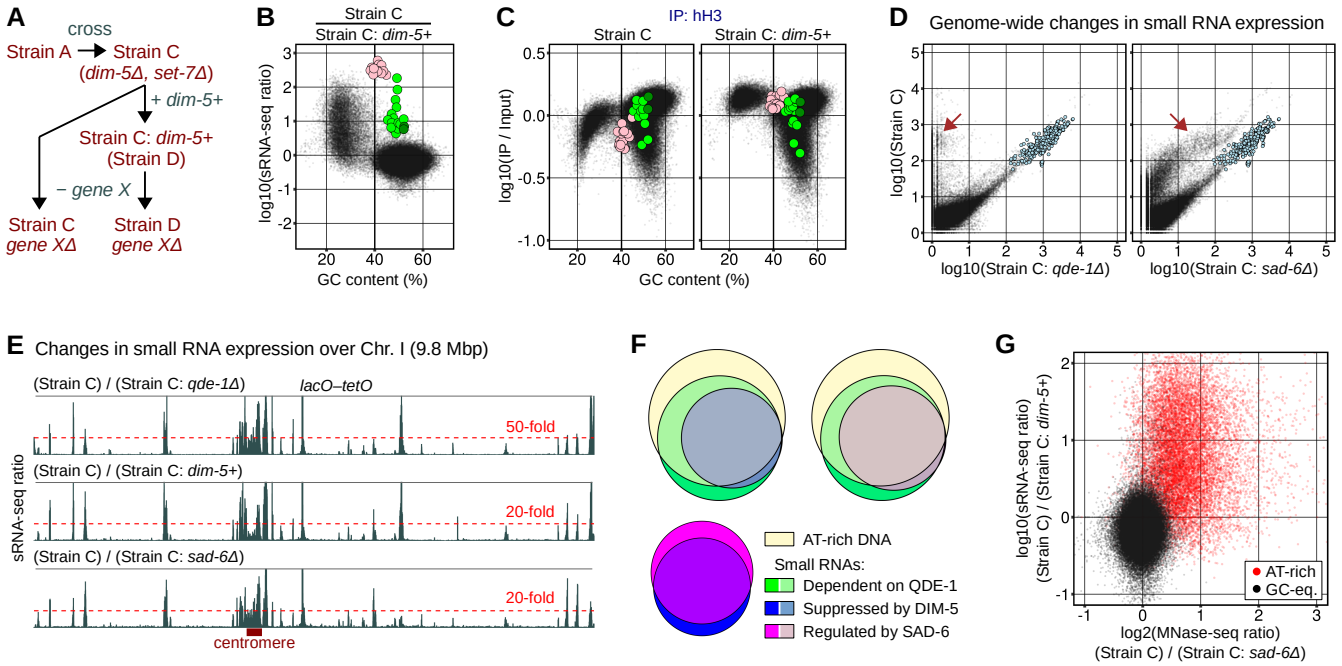
A
cross
Strain A
Strain C
(dim-5Δ, set-7Δ)
+ dim-5+
Strain C: dim-5+
(Strain D)
− gene X
Strain C
gene XΔ
Strain D
gene XΔ
B
Strain C
Strain C: dim-5+
log10(sRNA-seq ratio)
GC content (%)
C
IP: hH3
Strain C
Strain C: dim-5+
log10(IP / Input)
GC content (%)
D
Genome-wide changes in small RNA expression
log10(Strain C)
log10(Strain C: qde-1Δ)
log10(Strain C: sad-6Δ)
E
Changes in small RNA expression over Chr. I (9.8 Mbp)
(Strain C) / (Strain C: qde-1Δ)
lacO–tetO
50-fold
(Strain C) / (Strain C: dim-5+)
20-fold
(Strain C) / (Strain C: sad-6Δ)
20-fold
sRNA-seq ratio
centromere
F
AT-rich DNA
Small RNAs:
Dependent on QDE-1
Suppressed by DIM-5
Regulated by SAD-6
G
log10(sRNA-seq ratio)
(Strain C) / (Strain C: dim-5+)
log2(MNase-seq ratio)
(Strain C) / (Strain C: sad-6Δ)
AT-rich
GC-eq.

Figure 5

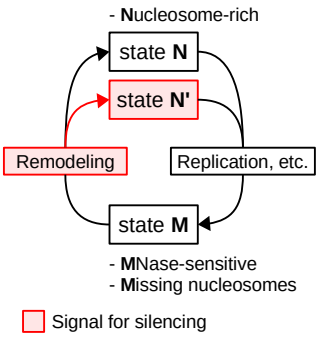
- Nucleosome-rich
state N
state N'
Remodeling
Replication, etc.
state M
- MNase-sensitive
- Missing nucleosomes
Signal for silencing

Figure 6

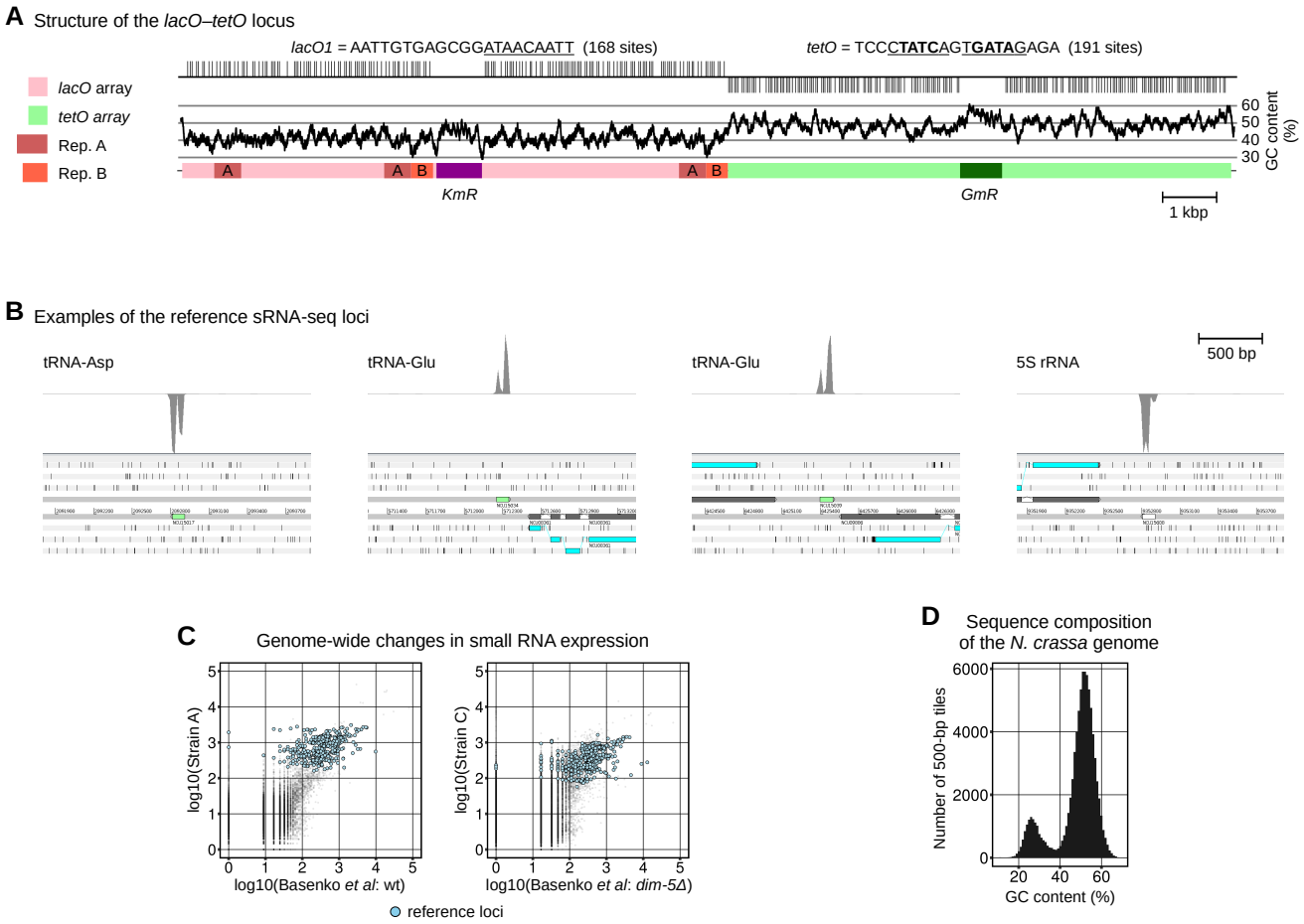
A Structure of the lacO–tetO locus
lacO1 = AATTGTGAGCGGATAACAATT (168 sites)
tetO = TCCCTATCAGTGATAGAGA (191 sites)
lacO array
tetO array
Rep. A
Rep. B
GC content (%)
KmR
GmR
1 kbp
B Examples of the reference sRNA-seq loci
tRNA-Asp
tRNA-Glu
tRNA-Glu
5S rRNA
500 bp
C Genome-wide changes in small RNA expression
log10(Strain A)
log10(Basenko et al: wt)
log10(Strain C)
log10(Basenko et al: dim-5Δ)
reference loci
D Sequence composition of the N. crassa genome
Number of 500-bp tiles
GC content (%)

Figure S1

A State of the *lacO–tetO* locus in several mutant strains derived from Strain B

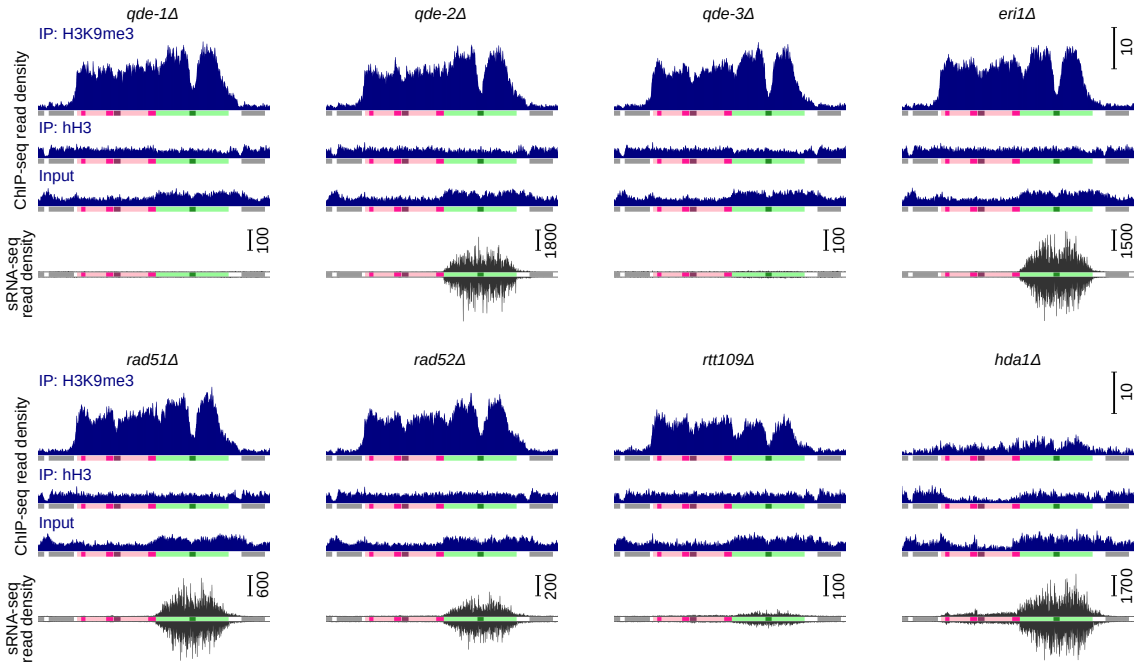

B

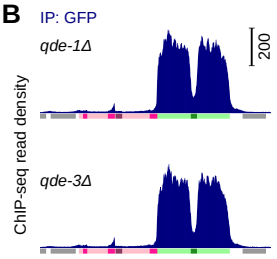

C

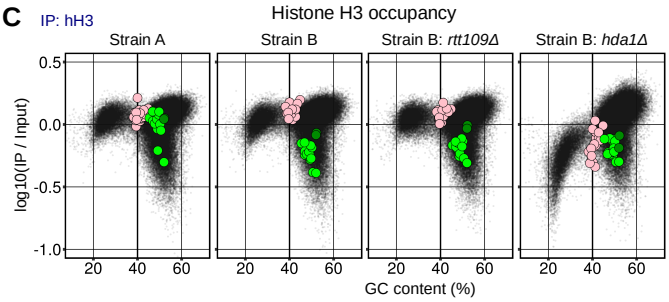

D Ratios of H3K9me3 enrichment (ChIP-seq reads, per 500 bp, per 1M mapped, also normalized by corresponding "Input" values)

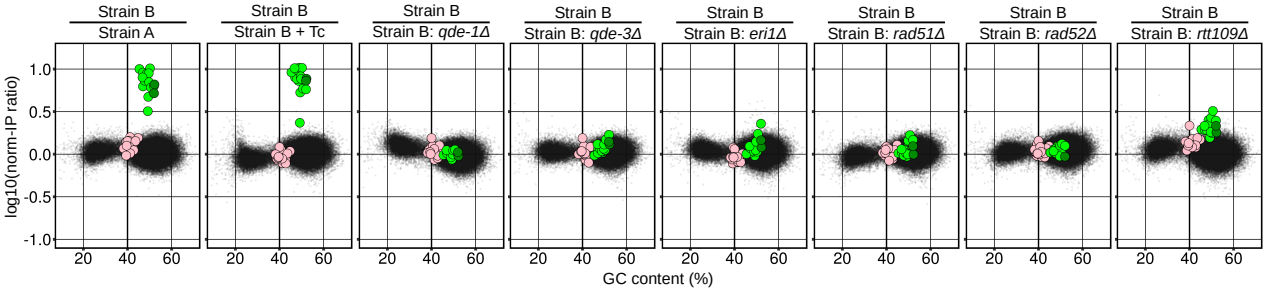

Figure S2

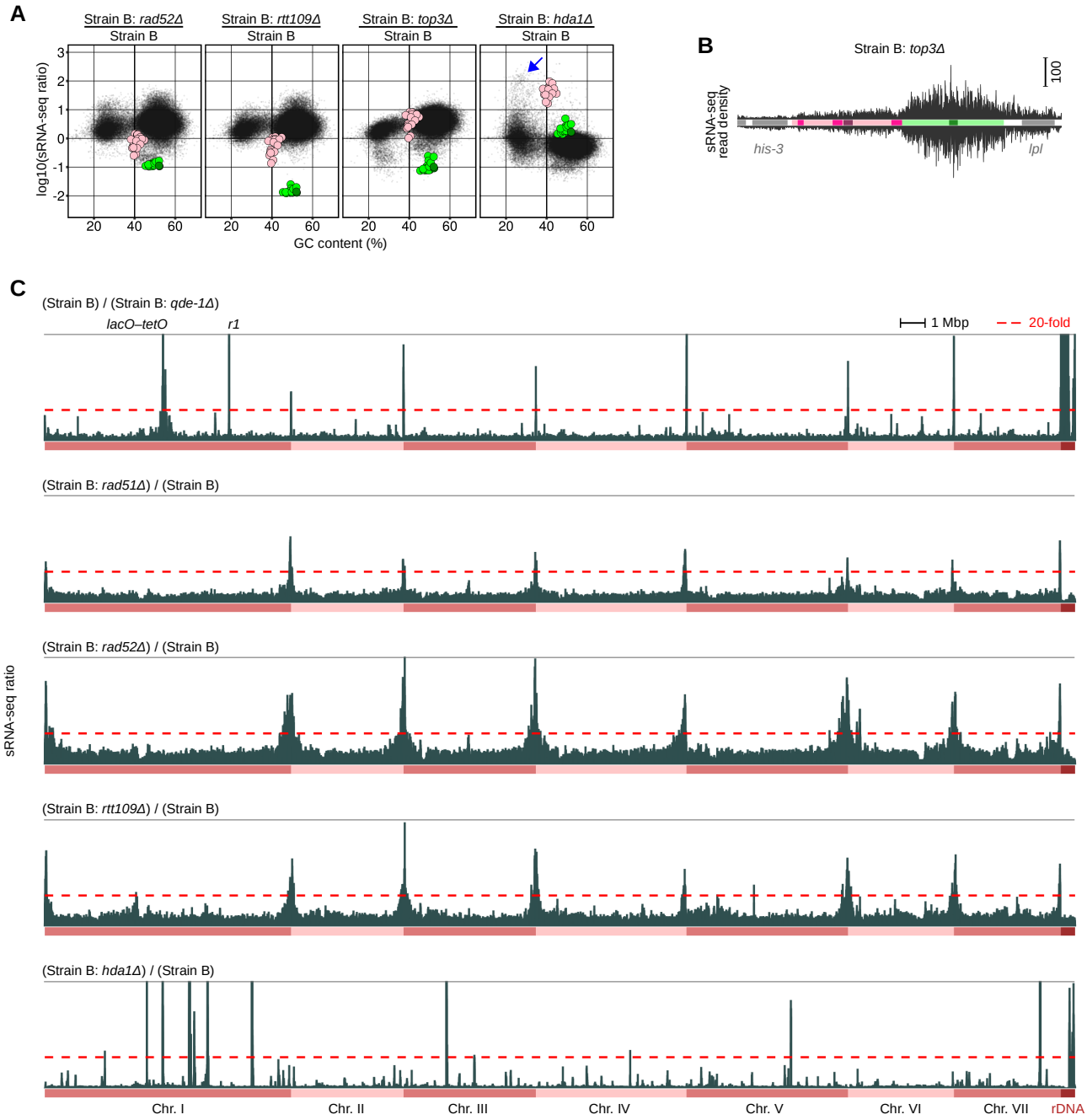
A
Strain B: rad52Δ
Strain B
Strain B: rtt109Δ
Strain B
Strain B: top3Δ
Strain B
Strain B: hda1Δ
Strain B
log10(sRNA-seq ratio)
GC content (%)
B
Strain B: top3Δ
sRNA-seq read density
100
his-3
lpl
C
(Strain B) / (Strain B: qde-1Δ)
lacO–tetO
r1
1 Mbp
20-fold
(Strain B: rad51Δ) / (Strain B)
(Strain B: rad52Δ) / (Strain B)
sRNA-seq ratio
(Strain B: rtt109Δ) / (Strain B)
(Strain B: hda1Δ) / (Strain B)
Chr. I
Chr. II
Chr. III
Chr. IV
Chr. V
Chr. VI
Chr. VII
rDNA

Figure S3

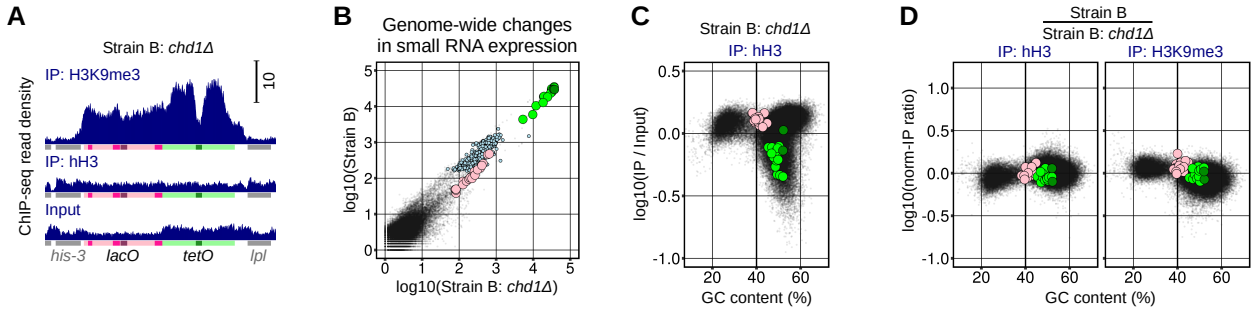
A
Strain B: chd1Δ
IP: H3K9me3
IP: hH3
Input
ChIP-seq read density
10
his-3
lacO
tetO
lpl
B
Genome-wide changes
in small RNA expression
log10(Strain B)
log10(Strain B: chd1Δ)
C
Strain B: chd1Δ
IP: hH3
log10(IP / Input)
GC content (%)
D
Strain B
Strain B: chd1Δ
IP: hH3
IP: H3K9me3
log10(norm-IP ratio)
GC content (%)

Figure S4

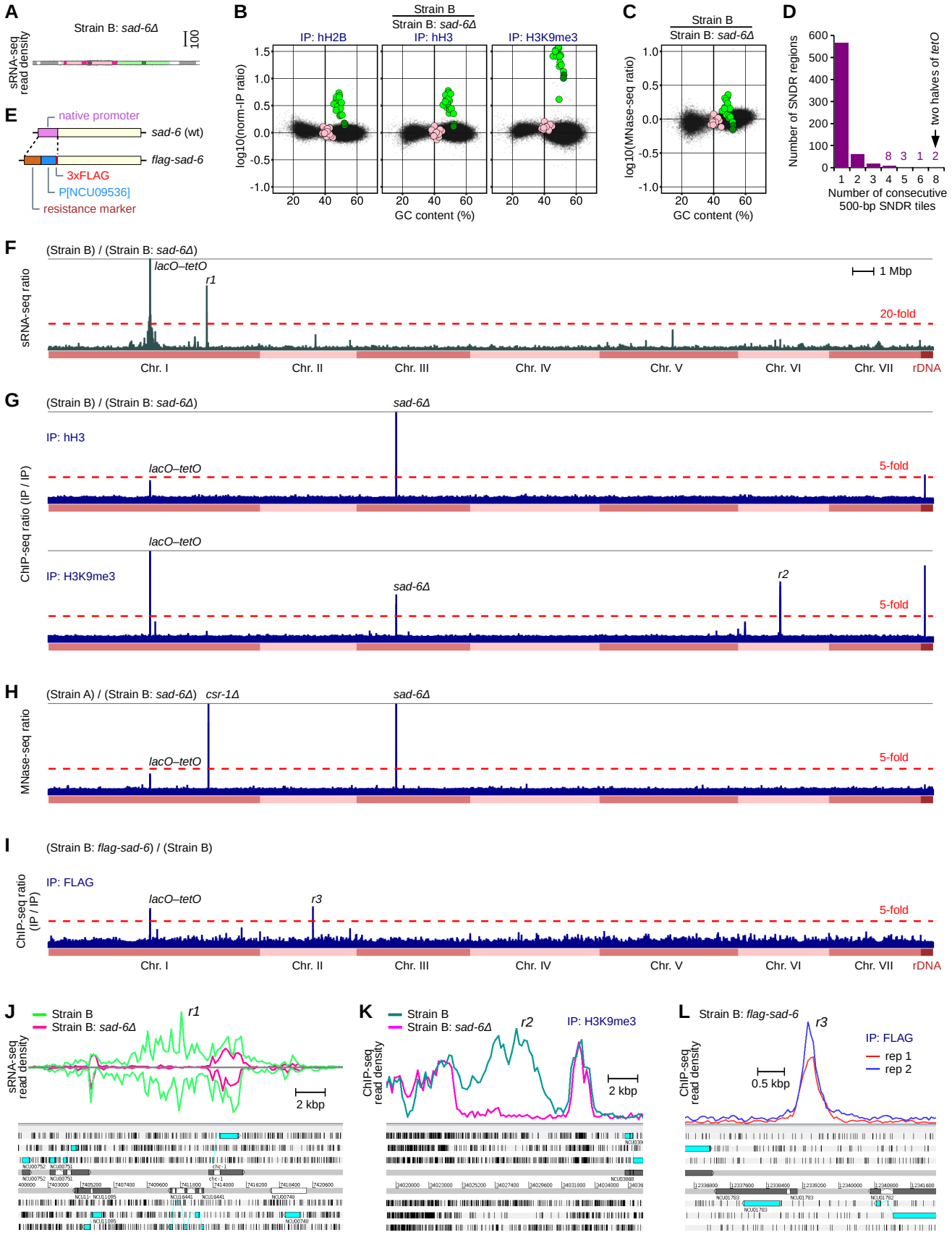
A
Strain B: sad-6Δ
sRNA-seq read density
100
B
Strain B
Strain B: sad-6Δ
IP: hH2B
IP: hH3
IP: H3K9me3
log10(norm-IP ratio)
GC content (%)
C
Strain B
Strain B: sad-6Δ
log10(MNase-seq ratio)
GC content (%)
D
Number of SNDR regions
two halves of tetO
8 3 1 2
Number of consecutive 500-bp SNDR tiles
E
native promoter
sad-6 (wt)
flag-sad-6
3xFLAG
P[NCU09536]
resistance marker
F
(Strain B) / (Strain B: sad-6Δ)
sRNA-seq ratio
lacO–tetO
r1
1 Mbp
20-fold
Chr. I
Chr. II
Chr. III
Chr. IV
Chr. V
Chr. VI
Chr. VII
rDNA
G
(Strain B) / (Strain B: sad-6Δ)
sad-6Δ
IP: hH3
lacO–tetO
5-fold
ChIP-seq ratio (IP / IP)
IP: H3K9me3
r2
H
(Strain A) / (Strain B: sad-6Δ)
csr-1Δ
MNase-seq ratio
I
(Strain B: flag-sad-6) / (Strain B)
IP: FLAG
r3
ChIP-seq ratio (IP / IP)
J
Strain B
Strain B: sad-6Δ
r1
sRNA-seq read density
2 kbp
K
Strain B
Strain B: sad-6Δ
r2
IP: H3K9me3
ChIP-seq read density
2 kbp
L
Strain B: flag-sad-6
r3
IP: FLAG
rep 1
rep 2
ChIP-seq read density
0.5 kbp

Figure S5

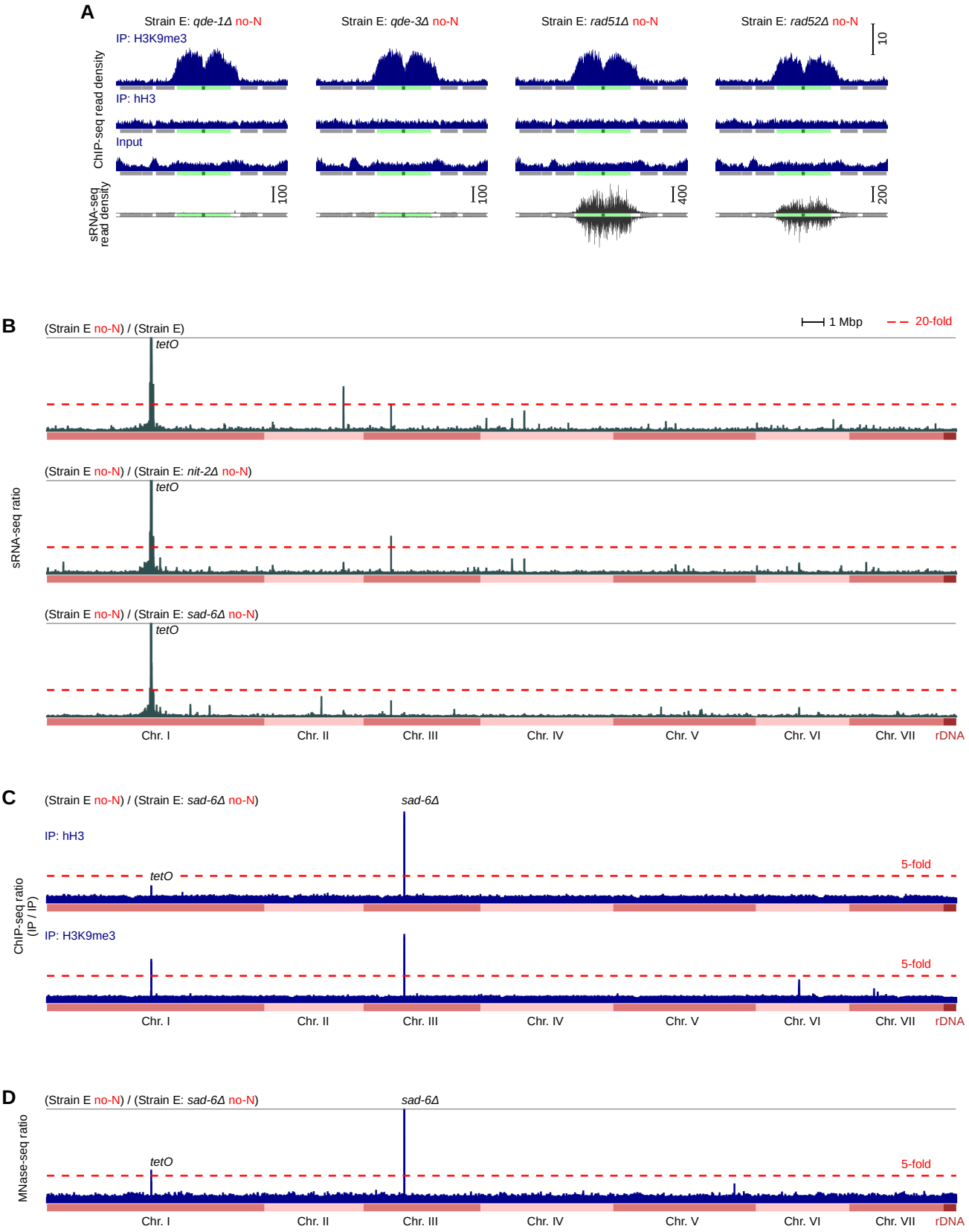
A
Strain E: qde-1Δ no-N
Strain E: qde-3Δ no-N
Strain E: rad51Δ no-N
Strain E: rad52Δ no-N
IP: H3K9me3
IP: hH3
Input
ChIP-seq read density
sRNA-seq read density
10
100
100
400
200
B
(Strain E no-N) / (Strain E)
(Strain E no-N) / (Strain E: nit-2Δ no-N)
(Strain E no-N) / (Strain E: sad-6Δ no-N)
1 Mbp
20-fold
tetO
sRNA-seq ratio
Chr. I
Chr. II
Chr. III
Chr. IV
Chr. V
Chr. VI
Chr. VII
rDNA
C
(Strain E no-N) / (Strain E: sad-6Δ no-N)
sad-6Δ
IP: hH3
IP: H3K9me3
tetO
5-fold
ChIP-seq ratio (IP / IP)
D
MNase-seq ratio

Figure S6

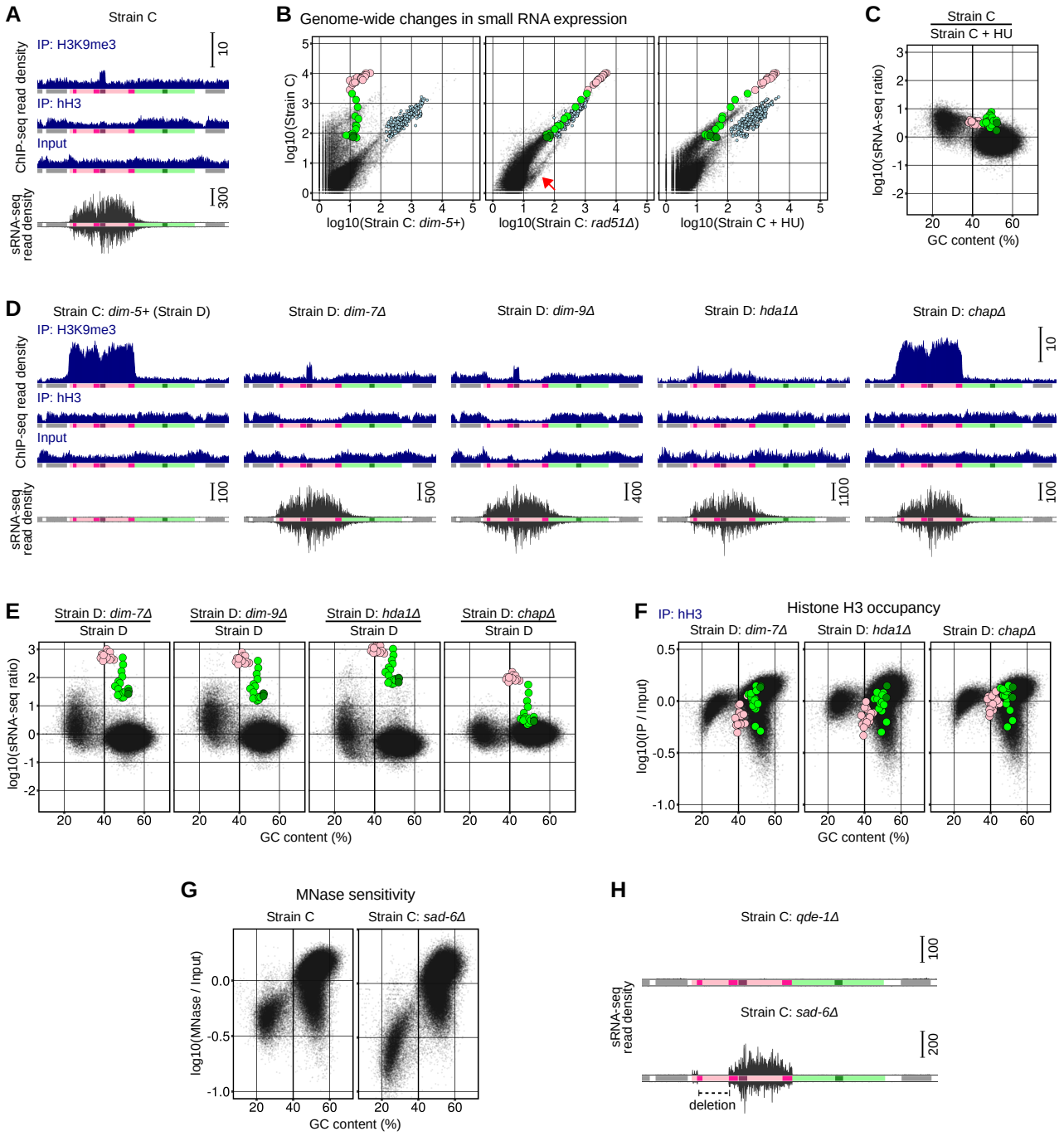
A
Strain C
IP: H3K9me3
IP: hH3
Input
ChIP-seq read density
sRNA-seq read density
10
300
B
Genome-wide changes in small RNA expression
log10(Strain C)
log10(Strain C: dim-5+)
log10(Strain C: rad51Δ)
log10(Strain C + HU)
C
Strain C
Strain C + HU
log10(sRNA-seq ratio)
GC content (%)
D
Strain C: dim-5+ (Strain D)
Strain D: dim-7Δ
Strain D: dim-9Δ
Strain D: hda1Δ
Strain D: chapΔ
IP: H3K9me3
IP: hH3
Input
ChIP-seq read density
sRNA-seq read density
10
100
500
400
1100
100
E
Strain D: dim-7Δ / Strain D
Strain D: dim-9Δ / Strain D
Strain D: hda1Δ / Strain D
Strain D: chapΔ / Strain D
log10(sRNA-seq ratio)
GC content (%)
F
IP: hH3
Histone H3 occupancy
Strain D: dim-7Δ
Strain D: hda1Δ
Strain D: chapΔ
log10(IP / Input)
GC content (%)
G
MNase sensitivity
Strain C
Strain C: sad-6Δ
log10(MNase / Input)
GC content (%)
H
Strain C: qde-1Δ
Strain C: sad-6Δ
sRNA-seq read density
100
200
deletion

Figure S7

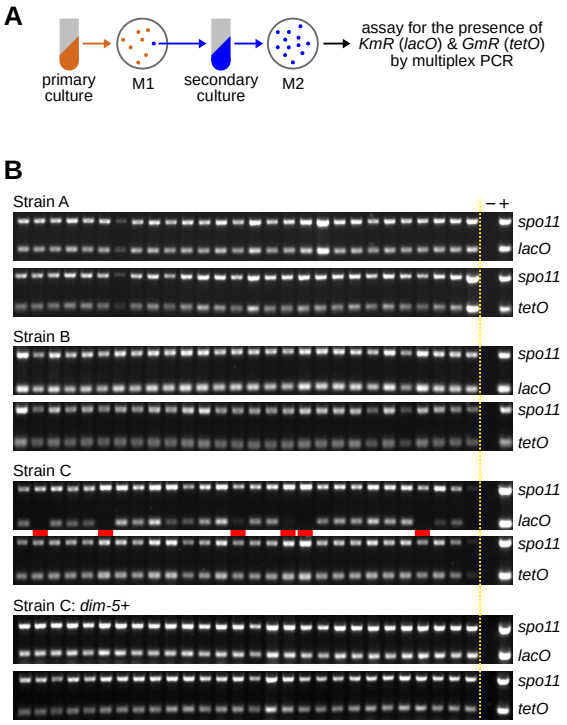
A
primary culture
M1
secondary culture
M2
assay for the presence of KmR (lacO) & GmR (tetO) by multiplex PCR
B
Strain A
− +
spo11
lacO
spo11
tetO
Strain B
spo11
lacO
spo11
tetO
Strain C
spo11
lacO
spo11
tetO
Strain C: dim-5+
spo11
lacO
spo11
tetO

Figure S8

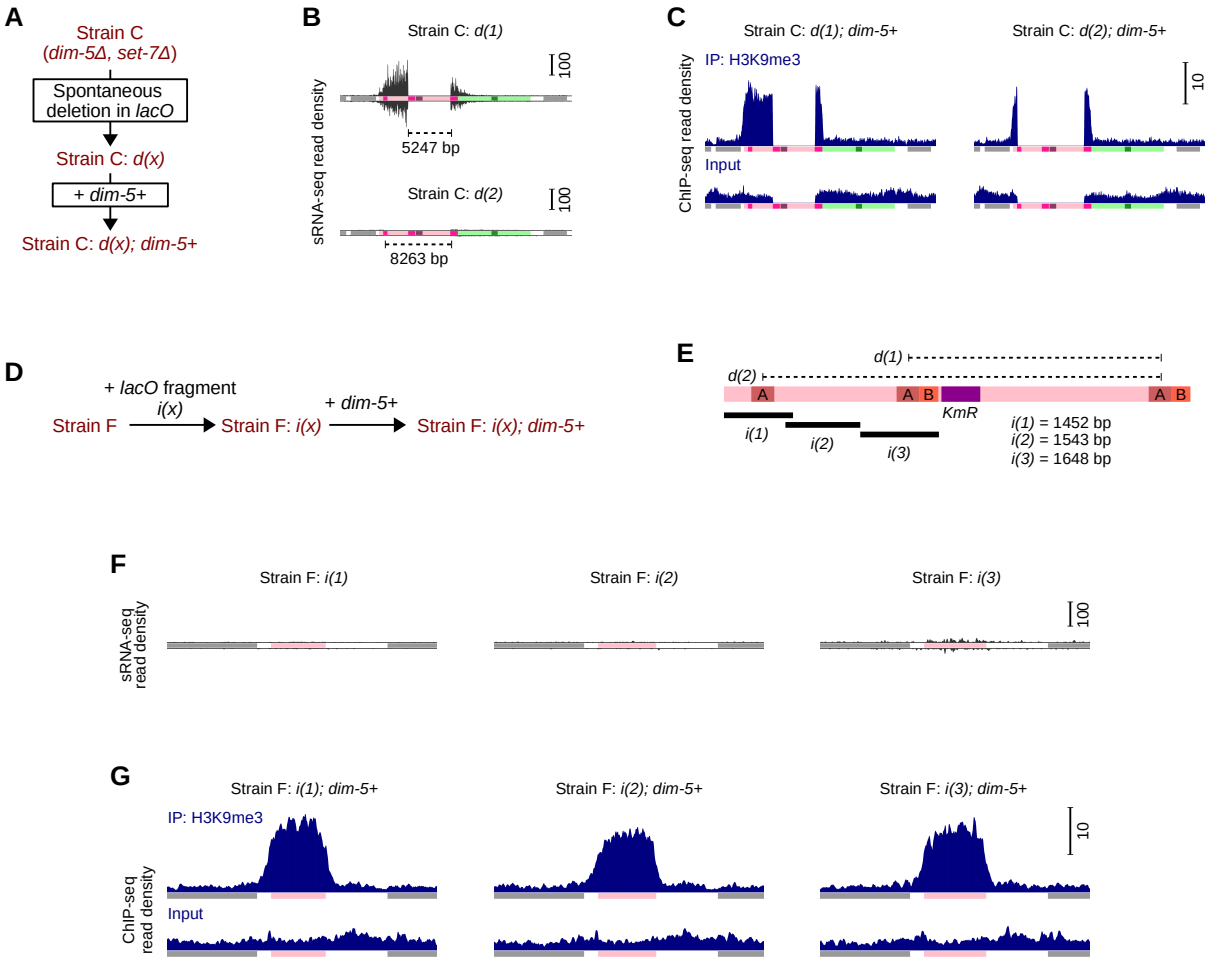
A
Strain C
(dim-5Δ, set-7Δ)
Spontaneous deletion in lacO
Strain C: d(x)
+ dim-5+
Strain C: d(x); dim-5+
B
Strain C: d(1)
sRNA-seq read density
100
5247 bp
Strain C: d(2)
100
8263 bp
C
Strain C: d(1); dim-5+
Strain C: d(2); dim-5+
IP: H3K9me3
ChIP-seq read density
10
Input
D
+ lacO fragment
i(x)
Strain F
Strain F: i(x)
+ dim-5+
Strain F: i(x); dim-5+
E
d(1)
d(2)
A
A B
A B
KmR
i(1)
i(2)
i(3)
i(1) = 1452 bp
i(2) = 1543 bp
i(3) = 1648 bp
F
Strain F: i(1)
Strain F: i(2)
Strain F: i(3)
sRNA-seq read density
100
G
Strain F: i(1); dim-5+
Strain F: i(2); dim-5+
Strain F: i(3); dim-5+
IP: H3K9me3
ChIP-seq read density
10
Input

Figure S9

Table S1. *Neurospora* genes analyzed in this study.

Gene	Standard ID	Synonym (if any)
chap	NCU01796	
chd1	NCU03060	*crf6-1*
csr-1	NCU00726	*cyp*
dim-2	NCU02247	
dim-5	NCU04402	*Su(var)3-9*
dim-7	NCU04152	
dim-9	NCU01656	
eri1	NCU06684	
hda1	NCU01525	
hh2b	NCU02435	*histone H2B*
hh3	NCU01635	*histone H3*
his-3	NCU03139	
lpl	NCU03141	
nit-2	NCU09068	*areA*
qde-1	NCU07534	
qde-2	NCU04730	
qde-3	NCU08598	*mus-19*
rad51	NCU02741	*mei-3*
rad52	NCU04275	*mus-11*
rid	NCU02034	
rtt109	NCU09825	
sad-6	NCU06190	*ATRX*
set-7	NCU07496	*E(z)*
spo11	NCU01120	
top3	NCU00081	

Table S2. *Neurospora* strains used in this study.

Strain	Internal ID	Genotype	Additional information
Strain O	**C58.7**	***a, ridΔ, dim-2Δ, mus-52Δ, his-3***	**DOI: 10.1038/ng.3857**
Strain A	T647.1h	C58.7 transformed with pFOC104A	
Strain B	T658.1	T647.1h transformed with pTSN7B	
Strain B: chd1Δ	T709.3h	T658.1 transformed with pFOC111B	
Strain B: eri1Δ	T770.2h	T658.1 transformed with pSCR8B	
Strain B: hda1Δ	T714.8h	T658.1 transformed with pFOC121B	
Strain B: qde-1Δ	T710.2h	T658.1 transformed with pFOC120B	
Strain B: qde-2Δ	T711.21h	T658.1 transformed with pFOC113B	
Strain B: qde-3Δ	T712.2h	T658.1 transformed with pFOC114B	
Strain B: rad51Δ	T737.1h	T658.1 transformed with pFOC106B	
Strain B: rad52Δ	T738.1h	T658.1 transformed with pFOC107B	
Strain B: rtt109Δ	T786.3h	T658.1 transformed with pFOC129B	
Strain B: sad-6Δ	T707.51h	T658.1 transformed with pFOC109B	
Strain B: flag-sad-6	T827.7h	T658.1 transformed with pFOC109N	
Strain B: top3Δ	T812.11h	T658.1 transformed with pSCR12B	
Strain E	T601.2h	C58.7 transformed with pTSN6	
Strain E: +tetR-gfp	T753.1	T601.2h transformed with pTSN7B	
Strain E: nit-2Δ	T851.1h	T601.2h transformed with pEAG276B	
Strain E: qde-1Δ	T839.10h	T601.2h transformed with pFOC120B	
Strain E: qde-3Δ	T840.10h	T601.2h transformed with pFOC114B	
Strain E: rad51Δ	T847.3h	T601.2h transformed with pFOC106B	
Strain E: rad52Δ	T848.1h	T601.2h transformed with pFOC107B	
Strain E: sad-6Δ	T774.4h	T601.2h transformed with pFOC109B	
Strain G	**C252.1**	***A, ridΔ, dim-2Δ, dim-5Δ, set-7Δ, sad-2Δ***	
Strain C	**C290.6**	***A, ridΔ, dim-2Δ, dim-5Δ, set-7Δ, mus-52Δ***	**Cross progeny of T647.1h & C252.1**
Strain C: d(1)	C290.6.C4	Clonal isolate of C290.6	
Strain C: d(2)	C290.6.C6	Clonal isolate of C290.6	
Strain C: d(1); dim-5+	T697.1	C290.6.C4 transformed with pEAG247A	
Strain C: d(2); dim-5+	T698.1	C290.6.C6 transformed with pEAG247A	
Strain C: dim-5+	T663.2	C290.6 transformed with pEAG247A	Strain D
Strain C: qde-1Δ	T739.4h	C290.6 transformed with pFOC120B	
Strain C: rad51Δ	T678.5h	C290.6 transformed with pFOC106B	
Strain C: sad-6Δ	T752.13h	C290.6 transformed with pFOC109B	
Strain D: chapΔ	T690.1h	T663.2 transformed with pFOC118B	
Strain D: dim-7Δ	T688.2h	T663.2 transformed with pFOC116B	
Strain D: dim-9Δ	T689.2h	T663.2 transformed with pFOC117B	
Strain D: hda1Δ	T743.3h	T663.2 transformed with pFOC121B	
Strain F	**C146.1**	***a, ridΔ, dim-5Δ, set-7Δ, mus-52Δ, his-3***	**DOI: 10.1038/ng.3857**
Strain F: i(1)	T724.2h	C146.1 transformed with pFOC125A	
Strain F: i(2)	T726.1h	C146.1 transformed with pFOC125C	
Strain F: i(3)	T728.1h	C146.1 transformed with pFOC125E	
Strain F: i(1); dim-5+	T764.1	T724.2h transformed with pEAG247A	
Strain F: i(2); dim-5+	T766.1	T726.1h transformed with pEAG247A	
Strain F: i(3); dim-5+	T776.1	T728.1h transformed with pEAG247A	

Table S3. Diagnostic primers used in this study.

Primer name	Internal name	Sequence
P1	HIS3_F4.2	GTGGATGTCACAATGTCCCT
P2	KMR_F1	ACATGGCAAAGGTAGCGTTG
P3	KMR_R1	TTCCGACTCGTCCAACATCA
P4	F104A_SEQ12	CAATTCGCGGCACAACTCTA
P5	F104A_SEQ14	TCTAGCAAGAGTGGGGATCC
P6	P62_SEQ3	TATAGAGAGCCACTGCGGGA
P7	P62_SEQ4	CCGTGGGTCGATGTTTGATG
P8	HIS3_R7	AGCGAACGAAACCCCTGAAAC
P9	SPO11_F	GTGTCGGAAGTCCCATTACCA
P10	SPO11_R	GTGACGCTGTGTAGTCGCTTG

Table S4. ChIP-seq libraries created and analyzed in this study.

#	Strain	Library ID	IP or Input	Alignment rate (%)	Aligned reads *	Paired Input Library ID	Condition
1	Strain A	CD397_i17_A	GFP	98.3	7929410	CD394_i14_A	
2	Strain A	CD593_i44_A	GFP	87.2	8976252	CD590_i48_A	
3	Strain A	CD2_i3_A	H3K9me3	96.5	5257486	CD1_i1_A	
4	Strain A	CD396_i16_A	H3K9me3	97.4	7609395	CD394_i14_A	
5	Strain A	CD8_i5_A	hH3	99.0	7766288	CD1_i1_A	
6	Strain A	CD395_i15_A	hH3	98.9	7798269	CD394_i14_A	
7	Strain A	CD1_i1_A	Input	99.0	5636932	N/A	
8	Strain A	CD394_i14_A	Input	99.0	8815831	N/A	
9	Strain A	CD590_i48_A	Input	99.0	11094748	N/A	
10	Strain B	CD669_i48_A	FLAG	96.2	8815307	CD529_i11_A	
11	Strain B	CD671_i47_A	FLAG	96.7	10365761	CD594_i27_A	
12	Strain B	CD463_i8_A	GFP	97.3	8909320	CD459_i43_A	Tc
13	Strain B	CD477_i10_A	GFP	98.7	6396447	CD473_i5_A	Tc
14	Strain B	CD28_i19_A	GFP	96.9	10006244	CD26_i17_A	
15	Strain B	CD221_i6_A	GFP	93.1	4276945	CD220_i5_A	
16	Strain B	CD461_i45_A	H3K9me3	97.3	8697139	CD459_i43_A	Tc
17	Strain B	CD475_i7_A	H3K9me3	97.2	6597607	CD473_i5_A	Tc
18	Strain B	CD29_i20_A	H3K9me3	97.6	10922524	CD26_i17_A	
19	Strain B	CD92_i43_A	H3K9me3	96.9	7653828	CD89_i40_A	
20	Strain B	CD731_i26_A	hH2B	99.0	9636938	CD459_i43_A	Tc
21	Strain B	CD732_i27_A	hH2B	99.0	9454969	CD473_i5_A	Tc
22	Strain B	CD729_i24_A	hH2B	98.8	9106248	CD529_i11_A	
23	Strain B	CD730_i25_A	hH2B	99.0	9851625	CD594_i27_A	
24	Strain B	CD460_i44_A	hH3	98.8	11649989	CD459_i43_A	Tc
25	Strain B	CD474_i6_A	hH3	99.0	6252061	CD473_i5_A	Tc
26	Strain B	CD27_i18_A	hH3	99.0	7549064	CD26_i17_A	
27	Strain B	CD90_i41_A	hH3	98.8	7775513	CD89_i40_A	
28	Strain B	CD459_i43_A	Input	99.1	15466837	N/A	Tc
29	Strain B	CD473_i5_A	Input	99.0	10379300	N/A	Tc
30	Strain B	CD26_i17_A	Input	99.0	6046340	N/A	
31	Strain B	CD89_i40_A	Input	98.9	8480540	N/A	
32	Strain B	CD220_i5_A	Input	98.7	7247386	N/A	
33	Strain B	CD529_i11_A	Input	98.9	8477778	N/A	
34	Strain B	CD594_i27_A	Input	98.8	9366140	N/A	
35	Strain B: chd1Δ	CD182_i20_A	H3K9me3	97.3	10597328	CD180_i18_A	
36	Strain B: chd1Δ	CD441_i25_A	H3K9me3	97.7	10717376	CD439_i23_A	
37	Strain B: chd1Δ	CD181_i19_A	hH3	81.4	8090865	CD180_i18_A	
38	Strain B: chd1Δ	CD440_i24_A	hH3	99.0	9477493	CD439_i23_A	
39	Strain B: chd1Δ	CD180_i18_A	Input	98.6	8172534	N/A	
40	Strain B: chd1Δ	CD439_i23_A	Input	99.2	8324205	N/A	
41	Strain B: eri1Δ	CD240_i22_A	H3K9me3	96.5	8209183	CD238_i20_A	
42	Strain B: eri1Δ	CD431_i15_A	H3K9me3	97.5	9112162	CD429_i13_A	
43	Strain B: eri1Δ	CD430_i14_A	hH3	99.1	7200067	CD429_i13_A	
44	Strain B: eri1Δ	CD239_i21_A	hH3	98.3	7230932	CD238_i20_A	

* Number of aligned reads is reported for the nuclear genome (corresponding to the interval 64841-41123470 in *mNC12.lacO-tetO*)

Table S4. ChIP-seq libraries created and analyzed in this study (continued).

45	Strain B: eri1Δ	CD429_i13_A	Input	99.0	8010217	N/A	
46	Strain B: eri1Δ	CD238_i20_A	Input	98.7	10293198	N/A	
47	Strain B: flag-sad-6	CD528_i32_A	FLAG	37.1	4506548	CD527_i4_A	Bl
48	Strain B: flag-sad-6	CD763_i33_A	FLAG	98.5	10738768	CD672_i46_A	Bl
49	Strain B: flag-sad-6	CD764_i34_A	FLAG	96.6	9150853	CD672_i46_A	Bl
50	Strain B: flag-sad-6	CD765_i35_A	FLAG	97.1	10576241	CD677_i41_A	Bl+Tc
51	Strain B: flag-sad-6	CD766_i36_A	FLAG	98.0	12321810	CD677_i41_A	Bl+Tc
52	Strain B: flag-sad-6	CD675_i43_A	GFP	97.9	10072417	CD672_i46_A	Bl
53	Strain B: flag-sad-6	CD604_i39_A	GFP	97.3	10537132	CD601_i43_A	Bl+Tc
54	Strain B: flag-sad-6	CD680_i38_A	GFP	98.4	10691467	CD677_i41_A	Bl+Tc
55	Strain B: flag-sad-6	CD674_i44_A	H3K9me3	96.8	10377412	CD672_i46_A	Bl
56	Strain B: flag-sad-6	CD799_i38_A	H3K9me3	91.3	5666258	CD527_i4_A	Bl
57	Strain B: flag-sad-6	CD603_i40_A	H3K9me3	97.6	9444811	CD601_i43_A	Bl+Tc
58	Strain B: flag-sad-6	CD679_i39_A	H3K9me3	97.3	10487142	CD677_i41_A	Bl+Tc
59	Strain B: flag-sad-6	CD673_i45_A	hH3	98.6	10431332	CD672_i46_A	Bl
60	Strain B: flag-sad-6	CD798_i37_A	hH3	98.8	7057779	CD527_i4_A	Bl
61	Strain B: flag-sad-6	CD602_i41_A	hH3	98.8	10748400	CD601_i43_A	Bl+Tc
62	Strain B: flag-sad-6	CD678_i40_A	hH3	98.8	10514385	CD677_i41_A	Bl+Tc
63	Strain B: flag-sad-6	CD527_i4_A	Input	98.9	10730984	N/A	Bl
64	Strain B: flag-sad-6	CD672_i46_A	Input	98.8	11006000	N/A	Bl
65	Strain B: flag-sad-6	CD601_i43_A	Input	98.9	10390350	N/A	Bl+Tc
66	Strain B: flag-sad-6	CD677_i41_A	Input	98.8	11240383	N/A	Bl+Tc
67	Strain B: hda1Δ	CD138_i34_A	H3K9me3	96.8	5320153	CD136_i17_A	
68	Strain B: hda1Δ	CD137_i19_A	hH3	99.1	7581904	CD136_i17_A	
69	Strain B: hda1Δ	CD136_i17_A	Input	98.9	7478362	N/A	
70	Strain B: qde-1Δ	CD424_i1_A	GFP	97.2	8583286	CD421_i5_A	
71	Strain B: qde-1Δ	CD435_i19_A	GFP	93.1	7774689	CD432_i16_A	
72	Strain B: qde-1Δ	CD423_i7_A	H3K9me3	97.3	7300690	CD421_i5_A	
73	Strain B: qde-1Δ	CD434_i18_A	H3K9me3	97.2	8452778	CD432_i16_A	
74	Strain B: qde-1Δ	CD422_i6_A	hH3	99.0	8298992	CD421_i5_A	
75	Strain B: qde-1Δ	CD433_i17_A	hH3	98.9	9519976	CD432_i16_A	
76	Strain B: qde-1Δ	CD421_i5_A	Input	99.0	8638738	N/A	
77	Strain B: qde-1Δ	CD432_i16_A	Input	99.0	7704419	N/A	
78	Strain B: qde-2Δ	CD196_i32_A	H3K9me3	96.6	7747370	CD194_i30_A	
79	Strain B: qde-2Δ	CD438_i22_A	H3K9me3	97.0	8674141	CD436_i20_A	
80	Strain B: qde-2Δ	CD195_i31_A	hH3	98.5	8368280	CD194_i30_A	
81	Strain B: qde-2Δ	CD437_i21_A	hH3	69.3	6663839	CD436_i20_A	
82	Strain B: qde-2Δ	CD194_i30_A	Input	98.5	8488470	N/A	
83	Strain B: qde-2Δ	CD436_i20_A	Input	99.1	9493385	N/A	
84	Strain B: qde-3Δ	CD428_i12_A	GFP	97.8	6900465	CD425_i9_A	
85	Strain B: qde-3Δ	CD445_i29_A	GFP	98.6	6917632	CD442_i26_A	
86	Strain B: qde-3Δ	CD129_i44_A	H3K9me3	96.8	8243938	CD127_i43_A	
87	Strain B: qde-3Δ	CD444_i28_A	H3K9me3	97.2	8428380	CD442_i26_A	
88	Strain B: qde-3Δ	CD427_i11_A	H3K9me3	97.4	6846737	CD425_i9_A	
89	Strain B: qde-3Δ	CD128_i15_A	hH3	98.8	7664057	CD127_i43_A	
90	Strain B: qde-3Δ	CD426_i10_A	hH3	99.1	7094939	CD425_i9_A	
91	Strain B: qde-3Δ	CD443_i27_A	hH3	97.3	8516563	CD442_i26_A	
92	Strain B: qde-3Δ	CD127_i43_A	Input	98.8	8261073	N/A	
93	Strain B: qde-3Δ	CD442_i26_A	Input	99.1	6015297	N/A	
94	Strain B: qde-3Δ	CD425_i9_A	Input	99.1	7512143	N/A	

Table S4. ChIP-seq libraries created and analyzed in this study (continued).

95	Strain B: rad51Δ	CD147_i41_A	H3K9me3	97.0	8337203	CD145_i39_A	
96	Strain B: rad51Δ	CD404_i24_A	H3K9me3	97.2	10136955	CD402_i22_A	
97	Strain B: rad51Δ	CD403_i23_A	hH3	99.0	9258535	CD402_i22_A	
98	Strain B: rad51Δ	CD762_i32_A	hH3	98.4	8957878	CD145_i39_A	
99	Strain B: rad51Δ	CD145_i39_A	Input	97.8	8378515	N/A	
100	Strain B: rad51Δ	CD402_i22_A	Input	98.9	9409013	N/A	
101	Strain B: rad52Δ	CD186_i24_A	H3K9me3	96.5	9324486	CD184_i22_A	
102	Strain B: rad52Δ	CD407_i27_A	H3K9me3	97.1	9284593	CD405_i25_A	
103	Strain B: rad52Δ	CD185_i23_A	hH3	98.5	8814243	CD184_i22_A	
104	Strain B: rad52Δ	CD406_i26_A	hH3	99.0	8800775	CD405_i25_A	
105	Strain B: rad52Δ	CD184_i22_A	Input	98.5	9206043	N/A	
106	Strain B: rad52Δ	CD405_i25_A	Input	99.0	9393715	N/A	
107	Strain B: rtt109Δ	CD377_i48_A	H3K9me3	95.6	6482608	CD375_i47_A	
108	Strain B: rtt109Δ	CD448_i32_A	H3K9me3	97.2	7149877	CD446_i30_A	
109	Strain B: rtt109Δ	CD376_i29_A	hH3	98.3	8275565	CD375_i47_A	
110	Strain B: rtt109Δ	CD447_i31_A	hH3	99.0	7456714	CD446_i30_A	
111	Strain B: rtt109Δ	CD375_i47_A	Input	98.7	7137760	N/A	
112	Strain B: rtt109Δ	CD446_i30_A	Input	99.1	7804782	N/A	
113	Strain B: sad-6Δ	CD458_i42_A	GFP	98.5	9891388	CD454_i38_A	Tc
114	Strain B: sad-6Δ	CD632_i6_A	GFP	98.8	8444453	CD629_i9_A	Tc
115	Strain B: sad-6Δ	CD262_i43_A	GFP	93.1	7346354	CD259_i40_A	
116	Strain B: sad-6Δ	CD401_i21_A	GFP	98.2	8513589	CD398_i18_A	
117	Strain B: sad-6Δ	CD456_i40_A	H3K9me3	98.1	10193635	CD454_i38_A	Tc
118	Strain B: sad-6Δ	CD631_i7_A	H3K9me3	97.4	9147582	CD629_i9_A	Tc
119	Strain B: sad-6Δ	CD261_i42_A	H3K9me3	97.0	8832346	CD259_i40_A	
120	Strain B: sad-6Δ	CD400_i20_A	H3K9me3	97.0	7928262	CD398_i18_A	
121	Strain B: sad-6Δ	CD736_i31_A	hH2B	99.0	8931671	CD454_i38_A	Tc
122	Strain B: sad-6Δ	CD737_i32_A	hH2B	98.9	7844732	CD629_i9_A	Tc
123	Strain B: sad-6Δ	CD733_i28_A	hH2B	98.9	9741353	CD398_i18_A	
124	Strain B: sad-6Δ	CD735_i30_A	hH2B	98.8	9109414	CD734_i29_A	
125	Strain B: sad-6Δ	CD455_i39_A	hH3	99.0	13205725	CD454_i38_A	Tc
126	Strain B: sad-6Δ	CD630_i8_A	hH3	98.8	9219792	CD629_i9_A	Tc
127	Strain B: sad-6Δ	CD260_i41_A	hH3	98.5	7870943	CD259_i40_A	
128	Strain B: sad-6Δ	CD399_i19_A	hH3	98.9	9548072	CD398_i18_A	
129	Strain B: sad-6Δ	CD454_i38_A	Input	99.2	11323585	N/A	Tc
130	Strain B: sad-6Δ	CD629_i9_A	Input	99.0	9775144	N/A	Tc
131	Strain B: sad-6Δ	CD259_i40_A	Input	98.8	12084203	N/A	
132	Strain B: sad-6Δ	CD398_i18_A	Input	99.0	10727138	N/A	
133	Strain B: sad-6Δ	CD734_i29_A	Input	98.8	8947082	N/A	
134	Strain C	CD69_i37_A	H3K9me3	98.4	7002290	CD67_i35_A	
135	Strain C	CD569_i45_A	H3K9me3	95.3	7793367	CD567_i48_A	
136	Strain C	CD68_i36_A	hH3	98.8	8373074	CD67_i35_A	
137	Strain C	CD568_i46_A	hH3	98.4	7145823	CD567_i48_A	
138	Strain C	CD67_i35_A	Input	98.4	8426641	N/A	
139	Strain C	CD567_i48_A	Input	98.5	8075101	N/A	
140	Strain C: d(1); dim-5+	CD61_i48_A	H3K9me3	97.8	5278648	CD60_i47_A	
141	Strain C: d(1); dim-5+	CD556_i36_A	H3K9me3	96.7	8153045	CD555_i37_A	
142	Strain C: d(1); dim-5+	CD60_i47_A	Input	99.3	6408038	N/A	
143	Strain C: d(1); dim-5+	CD555_i37_A	Input	99.0	9482890	N/A	
144	Strain C: d(2); dim-5+	CD66_i34_A	H3K9me3	88.5	7339481	CD65_i33_A	

Table S4. ChIP-seq libraries created and analyzed in this study (continued).

145	Strain C: d(2); dim-5+	CD558_i34_A	H3K9me3	96.5	6864519	CD557_i35_A	
146	Strain C: d(2); dim-5+	CD65_i33_A	Input	99.4	8631930	N/A	
147	Strain C: d(2); dim-5+	CD557_i35_A	Input	98.9	8147564	N/A	
148	Strain C: dim-5+	CD40_i27_A	H3K9me3	97.8	10427164	CD38_i25_A	
149	Strain C: dim-5+	CD769_i38_A	H3K9me3	95.0	9142215	CD294_i25_A	
150	Strain C: dim-5+	CD39_i26_A	hH3	99.0	7942226	CD38_i25_A	
151	Strain C: dim-5+	CD768_i37_A	hH3	98.9	10418247	CD294_i25_A	
152	Strain C: dim-5+	CD38_i25_A	Input	99.2	6976064	N/A	
153	Strain C: dim-5+	CD294_i25_A	Input	98.4	9361089	N/A	
154	Strain C: sad-6Δ	CD830_i29_A	hH3	98.7	8808509	CD829_i28_A	
155	Strain C: sad-6Δ	CD829_i28_A	Input	98.7	10053671	N/A	
156	Strain D: chapΔ	CD49_i36_A	H3K9me3	97.5	9337383	CD47_i34_A	
157	Strain D: chapΔ	CD579_i33_A	H3K9me3	97.2	8135547	CD577_i35_A	
158	Strain D: chapΔ	CD48_i35_A	hH3	99.2	8855879	CD47_i34_A	
159	Strain D: chapΔ	CD578_i34_A	hH3	98.6	7111554	CD577_i35_A	
160	Strain D: chapΔ	CD47_i34_A	Input	99.1	6600607	N/A	
161	Strain D: chapΔ	CD577_i35_A	Input	92.5	7972673	N/A	
162	Strain D: dim-7Δ	CD43_i30_A	H3K9me3	98.3	6777728	CD41_i28_A	
163	Strain D: dim-7Δ	CD573_i40_A	H3K9me3	94.2	8595604	CD571_i43_A	
164	Strain D: dim-7Δ	CD42_i29_A	hH3	99.2	11718495	CD41_i28_A	
165	Strain D: dim-7Δ	CD572_i41_A	hH3	98.5	7047100	CD571_i43_A	
166	Strain D: dim-7Δ	CD41_i28_A	Input	99.1	8792743	N/A	
167	Strain D: dim-7Δ	CD571_i43_A	Input	98.6	8428865	N/A	
168	Strain D: dim-9Δ	CD46_i33_A	H3K9me3	98.4	8255276	CD44_i31_A	
169	Strain D: dim-9Δ	CD576_i36_A	H3K9me3	96.9	9271303	CD574_i39_A	
170	Strain D: dim-9Δ	CD45_i32_A	hH3	99.2	9513255	CD44_i31_A	
171	Strain D: dim-9Δ	CD575_i38_A	hH3	98.8	9986908	CD574_i39_A	
172	Strain D: dim-9Δ	CD44_i31_A	Input	99.2	6616746	N/A	
173	Strain D: dim-9Δ	CD574_i39_A	Input	98.5	10005228	N/A	
174	Strain D: hda1Δ	CD135_i48_A	H3K9me3	97.1	6833539	CD133_i47_A	
175	Strain D: hda1Δ	CD134_i18_A	hH3	98.9	8831960	CD133_i47_A	
176	Strain D: hda1Δ	CD133_i47_A	Input	98.9	6330925	N/A	
177	Strain E	CD848_i36_A	H3K9me3	93.7	8643593	CD845_i33_A	"maintained"
178	Strain E	CD844_i42_A	H3K9me3	96.6	7761265	CD843_i41_A	"released"
179	Strain E	CD852_i4_A	H3K9me3	92.3	8634000	CD849_i1_A	"released"
180	Strain E	CD655_i37_A	H3K9me3	98.1	8476509	CD653_i35_A	no-N
181	Strain E	CD750_i25_A	H3K9me3	97.4	8908047	CD723_i18_A	no-N
182	Strain E	CD75_i43_A	H3K9me3	97.5	7793876	CD73_i41_A	
183	Strain E	CD652_i34_A	H3K9me3	98.5	8145259	CD650_i32_A	
184	Strain E	CD741_i36_A	hH2B	98.8	10530685	CD723_i18_A	no-N
185	Strain E	CD740_i35_A	hH2B	98.9	8585096	CD697_i24_A	no-N
186	Strain E	CD738_i33_A	hH2B	98.8	9637627	CD650_i32_A	
187	Strain E	CD739_i34_A	hH2B	99.0	8700628	CD721_i16_A	
188	Strain E	CD654_i36_A	hH3	96.3	7792030	CD653_i35_A	no-N
189	Strain E	CD698_i23_A	hH3	98.6	8852422	CD697_i24_A	no-N
190	Strain E	CD74_i42_A	hH3	99.1	8816753	CD73_i41_A	
191	Strain E	CD651_i33_A	hH3	99.1	8817367	CD650_i32_A	
192	Strain E	CD845_i33_A	Input	99.1	9926094	N/A	"maintained"
193	Strain E	CD843_i41_A	Input	98.9	9427679	N/A	"released"
194	Strain E	CD849_i1_A	Input	99.0	9054557	N/A	"released"

Table S4. ChIP-seq libraries created and analyzed in this study (continued).

195	Strain E	CD723_i18_A	Input	99.0	9226469	N/A	no-N
196	Strain E	CD697_i24_A	Input	99.0	8445763	N/A	no-N
197	Strain E	CD653_i35_A	Input	99.0	9196543	N/A	no-N
198	Strain E	CD650_i32_A	Input	98.6	9355163	N/A	
199	Strain E	CD721_i16_A	Input	98.9	11369712	N/A	
200	Strain E	CD73_i41_A	Input	98.0	9209709	N/A	
201	Strain E: +tetR-gfp	CD190_i28_A	H3K9me3	96.8	8798934	CD188_i26_A	
202	Strain E: +tetR-gfp	CD614_i30_A	H3K9me3	97.4	7039957	CD612_i32_A	
203	Strain E: +tetR-gfp	CD189_i27_A	hH3	98.5	8198700	CD188_i26_A	
204	Strain E: +tetR-gfp	CD613_i31_A	hH3	99.0	9640803	CD612_i32_A	
205	Strain E: +tetR-gfp	CD188_i26_A	Input	98.6	7988786	N/A	
206	Strain E: +tetR-gfp	CD612_i32_A	Input	98.9	11275351	N/A	
207	Strain E: nit-2Δ	CD667_i48_A	H3K9me3	98.4	8032158	CD665_i46_A	no-N
208	Strain E: nit-2Δ	CD690_i28_A	H3K9me3	96.3	9369072	CD688_i30_A	no-N
209	Strain E: nit-2Δ	CD666_i47_A	hH3	98.4	9158422	CD665_i46_A	no-N
210	Strain E: nit-2Δ	CD689_i29_A	hH3	98.4	9083438	CD688_i30_A	no-N
211	Strain E: nit-2Δ	CD665_i46_A	Input	99.1	10457276	N/A	no-N
212	Strain E: nit-2Δ	CD688_i30_A	Input	98.9	9823600	N/A	no-N
213	Strain E: qde-1Δ	CD608_i35_A	H3K9me3	88.5	10022605	CD606_i36_A	no-N
214	Strain E: qde-1Δ	CD711_i6_A	H3K9me3	98.2	6636860	CD709_i4_A	no-N
215	Strain E: qde-1Δ	CD607_i27_A	hH3	98.6	9631010	CD606_i36_A	no-N
216	Strain E: qde-1Δ	CD710_i5_A	hH3	98.8	8712589	CD709_i4_A	no-N
217	Strain E: qde-1Δ	CD606_i36_A	Input	98.9	12868225	N/A	no-N
218	Strain E: qde-1Δ	CD709_i4_A	Input	99.2	8851401	N/A	no-N
219	Strain E: qde-3Δ	CD611_i33_A	H3K9me3	97.7	10392870	CD609_i34_A	no-N
220	Strain E: qde-3Δ	CD752_i26_A	H3K9me3	97.7	9109045	CD715_i10_A	no-N
221	Strain E: qde-3Δ	CD610_i26_A	hH3	86.9	7683121	CD609_i34_A	no-N
222	Strain E: qde-3Δ	CD716_i11_A	hH3	99.0	7553969	CD715_i10_A	no-N
223	Strain E: qde-3Δ	CD715_i10_A	Input	99.2	9094349	N/A	no-N
224	Strain E: qde-3Δ	CD609_i34_A	Input	99.1	10277658	N/A	no-N
225	Strain E: rad51Δ	CD708_i3_A	H3K9me3	77.4	5436037	CD706_i1_A	no-N
226	Strain E: rad51Δ	CD754_i27_A	H3K9me3	97.8	8943634	CD700_i21_A	no-N
227	Strain E: rad51Δ	CD701_i20_A	hH3	99.0	9300497	CD700_i21_A	no-N
228	Strain E: rad51Δ	CD707_i2_A	hH3	97.7	8549931	CD706_i1_A	no-N
229	Strain E: rad51Δ	CD700_i21_A	Input	99.0	10417937	N/A	no-N
230	Strain E: rad51Δ	CD706_i1_A	Input	99.1	7828349	N/A	no-N
231	Strain E: rad52Δ	CD714_i9_A	H3K9me3	97.0	7071655	CD712_i7_A	no-N
232	Strain E: rad52Δ	CD756_i28_A	H3K9me3	97.7	9872070	CD703_i18_A	no-N
233	Strain E: rad52Δ	CD704_i17_A	hH3	98.5	9440003	CD703_i18_A	no-N
234	Strain E: rad52Δ	CD713_i8_A	hH3	98.8	7385596	CD712_i7_A	no-N
235	Strain E: rad52Δ	CD703_i18_A	Input	99.0	8137387	N/A	no-N
236	Strain E: rad52Δ	CD712_i7_A	Input	99.0	8000728	N/A	no-N
237	Strain E: sad-6Δ	CD658_i40_A	H3K9me3	97.7	9927567	CD656_i38_A	no-N
238	Strain E: sad-6Δ	CD687_i31_A	H3K9me3	96.5	9708825	CD685_i33_A	no-N
239	Strain E: sad-6Δ	CD745_i40_A	hH2B	98.9	7706122	CD685_i33_A	no-N
240	Strain E: sad-6Δ	CD746_i41_A	hH2B	98.7	7986318	CD727_i22_A	no-N
241	Strain E: sad-6Δ	CD742_i37_A	hH2B	99.0	10163595	CD725_i20_A	
242	Strain E: sad-6Δ	CD744_i39_A	hH2B	98.8	9149919	CD743_i38_A	
243	Strain E: sad-6Δ	CD657_i39_A	hH3	98.5	9787164	CD656_i38_A	no-N
244	Strain E: sad-6Δ	CD686_i32_A	hH3	98.5	9187849	CD685_i33_A	no-N

Table S4. ChIP-seq libraries created and analyzed in this study (continued).

245	Strain E: sad-6Δ	CD685_i33_A	Input	98.9	8575543	N/A	no-N
246	Strain E: sad-6Δ	CD656_i38_A	Input	99.0	9538401	N/A	no-N
247	Strain E: sad-6Δ	CD727_i22_A	Input	99.0	8307630	N/A	no-N
248	Strain E: sad-6Δ	CD725_i20_A	Input	98.9	9546376	N/A	
249	Strain E: sad-6Δ	CD743_i38_A	Input	98.4	9014884	N/A	
250	Strain F: i(1); dim-5+	CD202_i38_A	H3K9me3	96.9	7305893	CD201_i37_A	
251	Strain F: i(1); dim-5+	CD562_i30_A	H3K9me3	96.8	9060889	CD561_i31_A	
252	Strain F: i(1); dim-5+	CD201_i37_A	Input	98.5	6529896	N/A	
253	Strain F: i(1); dim-5+	CD561_i31_A	Input	98.8	10258869	N/A	
254	Strain F: i(2); dim-5+	CD204_i40_A	H3K9me3	96.1	5680629	CD203_i39_A	
255	Strain F: i(2); dim-5+	CD564_i28_A	H3K9me3	96.6	8147239	CD563_i29_A	
256	Strain F: i(2); dim-5+	CD203_i39_A	Input	98.4	8587633	N/A	
257	Strain F: i(2); dim-5+	CD563_i29_A	Input	98.5	8521230	N/A	
258	Strain F: i(3); dim-5+	CD206_i42_A	H3K9me3	96.7	6528076	CD205_i41_A	
259	Strain F: i(3); dim-5+	CD566_i42_A	H3K9me3	97.2	7423559	CD565_i47_A	
260	Strain F: i(3); dim-5+	CD205_i41_A	Input	98.6	5535835	N/A	
261	Strain F: i(3); dim-5+	CD565_i47_A	Input	98.9	8428602	N/A	

Table S5. MNase-seq libraries created and analyzed in this study.

Strain / Condition	Library ID	Alignment rate (%)	Aligned reads *
Strain A	CD1072_i0_A	99.3	26796362
Strain B	CD530_i12_A	99.1	10769647
Strain B: sad-6Δ	CD533_i15_A	99.0	12371585
Strain C	CD290_i21_A	98.5	11797272
Strain C: sad-6Δ	CD832_i30_A	99.2	12764340
Strain E no-N	CD587_i15_A	99.2	15232062
Strain E: sad-6Δ no-N	CD589_i14_A	99.3	14815243

* Number of aligned reads is reported for the nuclear genome (corresponding to the interval 64841-41123470 in *mNC12.lacO-tetO*)

Table S6. sRNA-seq libraries created and analyzed in this study.

#	Strain	Library ID	Alignment rate (%)	Mitochondrial reads	Ribosomal reads	Core nuclear reads	Condition
1	Strain A	VR18_i16_A	91.5	89140	6334645	768640	
2	Strain A	VR167_i2_A	94.5	273129	4821765	1112917	
3	Strain B	VR13_i11_A	94.7	72864	3349707	669524	
4	Strain B	VR200_i19_A	95.1	354937	6246084	2046200	
5	Strain B	VR259_i47_A	92.6	330465	4767444	1953046	Bl
6	Strain B	VR274_i37_A	95.3	397237	6514549	2298582	Bl
7	Strain B	VR48_i25_A	93.6	1591285	3207673	923786	HU
8	Strain B	VR202_i21_A	94.3	1523622	4343824	2032401	HU
9	Strain B	VR201_i20_A	95.9	283061	6067766	1137260	Tc
10	Strain B	VR232_i43_A	95.0	100545	7477216	1011309	Tc
11	Strain B: chd1Δ	VR181_i9_A	95.1	365062	5327883	2700055	
12	Strain B: chd1Δ	VR234_i45_A	95.0	228614	4714202	1942622	
13	Strain B: eri1Δ	VR156_i18_A	93.7	208510	3976531	2827441	
14	Strain B: eri1Δ	VR226_i43_A	94.6	168717	5107627	2397763	
15	Strain B: flag-sad-6	VR275_i38_A	95.2	362259	6686193	1841027	Bl
16	Strain B: flag-sad-6	VR328_i0_A	86.5	140179	4821635	969352	Bl
17	Strain B: hda1Δ	VR67_i20_A	96.4	117222	1653395	4463222	
18	Strain B: hda1Δ	VR187_i5_A	93.3	180826	2141171	5662706	
19	Strain B: qde-1Δ	VR51_i28_A	94.1	199541	5057507	1055664	
20	Strain B: qde-1Δ	VR158_i20_A	93.8	337753	5208452	1259318	
21	Strain B: qde-2Δ	VR159_i21_A	91.0	176974	3485602	2274100	
22	Strain B: qde-2Δ	VR206_i25_A	90.5	352184	6498566	3417528	
23	Strain B: qde-3Δ	VR75_i33_A	96.0	175742	4122871	622478	
24	Strain B: qde-3Δ	VR207_i26_A	90.3	177939	5426733	786112	
25	Strain B: rad51Δ	VR182_i46_A	94.9	272390	5804726	3582359	
26	Strain B: rad51Δ	VR219_i36_A	93.3	285179	7066045	2967365	
27	Strain B: rad52Δ	VR178_i42_A	95.2	234040	3694120	7134007	
28	Strain B: rad52Δ	VR210_i29_A	94.0	213286	3682292	4382441	
29	Strain B: rtt109Δ	VR213_i32_A	94.0	127733	6865730	1343029	
30	Strain B: rtt109Δ	VR221_i38_A	94.4	171898	6281191	1998765	
31	Strain B: sad-6Δ	VR157_i19_A	92.4	384973	5419815	1623912	
32	Strain B: sad-6Δ	VR204_i23_A	95.4	305828	5999418	905752	
33	Strain B: top3Δ	VR242_i42_A	95.8	175430	3631633	4186739	
34	Strain B: top3Δ	VR246_i46_A	94.8	122062	5173798	2023411	
35	Strain C	VR139_i1_A	94.0	270021	5810093	2915944	
36	Strain C	VR195_i14_A	90.4	192356	3984691	2252637	
37	Strain C	VR15_i13_A	88.9	598556	2738413	756356	HU
38	Strain C	VR199_i18_A	93.8	296056	5583631	1021777	HU
39	Strain C: d(1)	VR4_i3_A	95.4	101949	3745549	961248	
40	Strain C: d(1)	VR264_i27_A	96.5	248698	6752046	2180782	
41	Strain C: d(2)	VR5_i28_A	92.3	124222	3910687	1078488	
42	Strain C: d(2)	VR265_i28_A	93.8	334516	6952769	3550683	
43	Strain C: dim-5+	VR1_i27_A	96.3	176973	5096301	894206	
44	Strain C: dim-5+	VR140_i2_A	95.2	323739	9390098	1655988	

Table S6. sRNA-seq libraries created and analyzed in this study (continued).

45	Strain C: qde-1Δ	VR52_i29_A	96.3	167825	5736656	849642	
46	Strain C: qde-1Δ	VR170_i34_A	94.6	63998	8986893	962974	
47	Strain C: qde-1Δ	VR368_i2_A	97.9	254400	22662127	2471385	
48	Strain C: rad51Δ	VR27_i23_A	95.2	186305	6174654	2362345	
49	Strain C: rad51Δ	VR41_i18_A	90.0	62074	2358548	1006793	
50	Strain C: rad51Δ	VR177_i41_A	94.3	215374	4479746	5634639	
51	Strain C: sad-6Δ	VR255_i39_A	96.1	153384	9522494	1376775	
52	Strain C: sad-6Δ	VR260_i48_A	95.9	143268	7577198	1006200	
53	Strain D: chapΔ	VR186_i26_A	91.5	830143	4924184	2136729	
54	Strain D: chapΔ	VR198_i17_A	94.7	166768	5612364	1034516	
55	Strain D: dim-7Δ	VR6_i4_A	96.5	161363	5416165	1501359	
56	Strain D: dim-7Δ	VR143_i5_A	94.2	185216	7371866	2690269	
57	Strain D: dim-9Δ	VR7_i5_A	95.5	119282	3553738	1260019	
58	Strain D: dim-9Δ	VR266_i29_A	95.3	225356	7131021	2355417	
59	Strain D: hda1Δ	VR62_i13_A	94.1	85391	1872060	2123860	
60	Strain D: hda1Δ	VR179_i43_A	93.4	209183	4538707	4005878	
61	Strain E	VR166_i30_A	94.5	435793	6926994	1351635	
62	Strain E	VR347_i0_A	93.0	304726	12151367	1691174	
63	Strain E	VR304_i23_A	95.2	312596	7185662	2676606	no-N
64	Strain E	VR308_i1_A	94.5	384311	6889801	1990153	no-N
65	Strain E	VR280_i43_A	94.3	176832	4934667	894476	N+ control
66	Strain E	VR350_i48_A	93.8	46571	4022817	559369	N+ control
67	Strain E	VR353_i46_A	94.2	134854	5476783	813063	N+ control
68	Strain E	VR314_i7_A	94.3	678899	9254058	1398482	"released"
69	Strain E	VR315_i8_A	94.0	330082	7129312	1850101	"maintained"
70	Strain E: +tetR-gfp	VR180_i44_A	89.2	231596	8574884	2001104	
71	Strain E: +tetR-gfp	VR208_i27_A	93.8	256389	6289769	2410247	
72	Strain E: nit-2Δ	VR329_i0_A	93.2	290039	8427720	1701623	no-N
73	Strain E: nit-2Δ	VR330_i0_A	94.5	250838	8409414	1660895	no-N
74	Strain E: nit-2Δ	VR344_i5_A	95.4	194513	6910524	1270996	no-N
75	Strain E: qde-1Δ	VR312_i0_A	95.4	889847	17261386	2543135	no-N
76	Strain E: qde-1Δ	VR316_i0_A	95.1	521087	11517703	1726187	no-N
77	Strain E: qde-3Δ	VR313_i0_A	95.1	917304	16945619	2790338	no-N
78	Strain E: qde-3Δ	VR317_i0_A	95.2	746121	12363669	2086566	no-N
79	Strain E: rad51Δ	VR331_i3_B	94.2	181149	3410221	2840787	no-N
80	Strain E: rad51Δ	VR332_i4_C	94.3	245869	5105236	4387030	no-N
81	Strain E: rad52Δ	VR333_i5_B	92.9	129785	3427957	2487608	no-N
82	Strain E: rad52Δ	VR334_i6_B	90.7	103778	3446758	1789739	no-N
83	Strain E: sad-6Δ	VR302_i0_A	94.6	397546	10630045	1666933	no-N
84	Strain E: sad-6Δ	VR348_i0_A	95.0	431348	12883573	2143730	no-N
85	Strain F: i(1)	VR76_i4_A	91.1	121473	3805143	899079	
86	Strain F: i(1)	VR189_i7_A	90.8	272686	3757672	2319565	
87	Strain F: i(2)	VR80_i8_A	93.5	132936	3561318	1139354	
88	Strain F: i(2)	VR191_i10_A	91.8	467307	4934028	2998980	
89	Strain F: i(3)	VR81_i25_A	85.6	62911	3848337	583177	